Cell Stem Cell

3D bioprinting of human neural tissues with functional connectivity

Graphical abstract

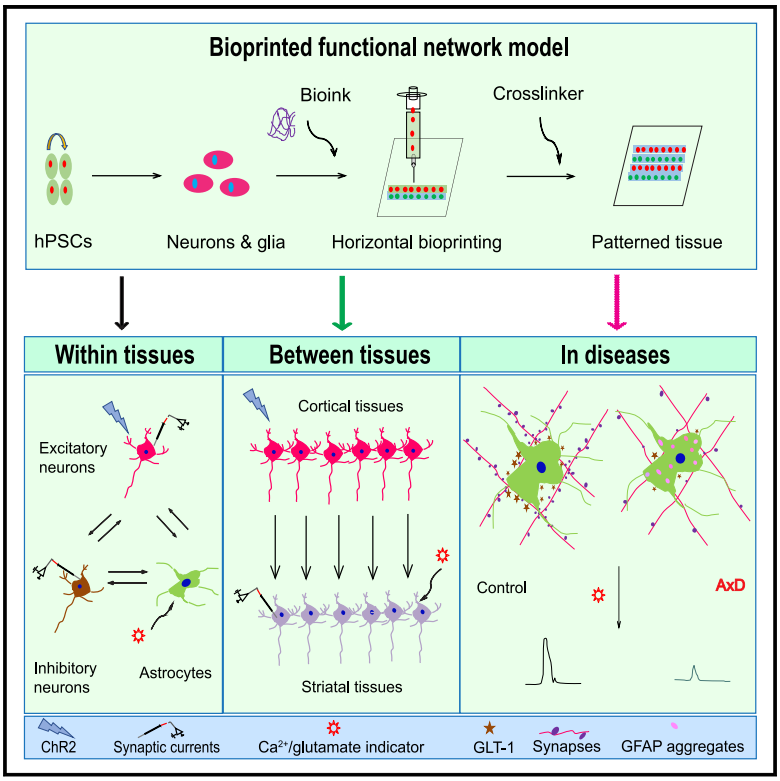

Authors

Yuanwei Yan, Xueyan Li, Yu Gao, ..., Anita Bhattacharyya, Xinyu Zhao, Su-Chun Zhang

Correspondence

suchun.zhang@wisc.edu

In brief

Yan et al. generate 3D bioprinted human brain tissues that form functional neural networks within and between tissues, providing an effective tool for modeling network activity under physiological and pathological conditions.

Highlights

- Functional human neural tissues assembled by 3D bioprinting
- Neural circuits formed between defined neural subtypes
- Functional connections established between cortical-striatal tissues
- Printed tissues for modeling neural network impairment

Yan et al., 2024, Cell Stem Cell *31*, 260–274
February 1, 2024
https://doi.org/10.1016/j.stem.2023.12.009

CellPress

CellPress
OPEN ACCESS

Cell Stem Cell

Technology

3D bioprinting of human neural tissues with functional connectivity

Yuanwei Yan,[1,9] Xueyan Li,[1,9] Yu Gao,[1] Sakthikumar Mathivanan,[1,8] Linghai Kong,[1] Yunlong Tao,[1,7,8] Yi Dong,[1] Xiang Li,[1] Anita Bhattacharyya,[1,2] Xinyu Zhao,[1,3] and Su-Chun Zhang[1,3,4,5,6,8,10,*]

[1]Waisman Center, University of Wisconsin-Madison, Madison, WI, USA
[2]Department of Cell and Regenerative Biology, School of Medicine and Public Health, University of Wisconsin, Madison, WI, USA
[3]Department of Neuroscience, School of Medicine and Public Health, University of Wisconsin, Madison, WI, USA
[4]Department of Neurology, School of Medicine and Public Health, University of Wisconsin, Madison, WI, USA
[5]Program in Neuroscience and Behavioral Disorders, Duke-NUS Medical School, Singapore, Singapore
[6]GK Goh Centre for Neuroscience, Duke-NUS Medical School, Singapore, Singapore
[7]State Key Laboratory of Pharmaceutical Biotechnology, School of Life Sciences, Chemistry and Biomedicine Innovation Center (ChemBIC), Nanjing University, Nanjing, China
[8]Aligning Science Across Parkinson's (ASAP) Collaborative Research Network, Chevy Chase, MD, 20815
[9]These authors contributed equally
[10]Lead contact
*Correspondence: suchun.zhang@wisc.edu
https://doi.org/10.1016/j.stem.2023.12.009

SUMMARY

Probing how human neural networks operate is hindered by the lack of reliable human neural tissues amenable to the dynamic functional assessment of neural circuits. We developed a 3D bioprinting platform to assemble tissues with defined human neural cell types in a desired dimension using a commercial bioprinter. The printed neuronal progenitors differentiate into neurons and form functional neural circuits within and between tissue layers with specificity within weeks, evidenced by the cortical-to-striatal projection, spontaneous synaptic currents, and synaptic response to neuronal excitation. Printed astrocyte progenitors develop into mature astrocytes with elaborated processes and form functional neuron-astrocyte networks, indicated by calcium flux and glutamate uptake in response to neuronal excitation under physiological and pathological conditions. These designed human neural tissues will likely be useful for understanding the wiring of human neural networks, modeling pathological processes, and serving as platforms for drug testing.

INTRODUCTION

The human brain is formed by the integration of specialized neuronal and glial types that are precisely wired into networks. Understanding how the human neural networks operate is essential to probing the health and disease of our brain. Animal models cannot precisely recapitulate the high-order information processing of the human brain due to the differences in neuronal composition, synaptic integration, astrocytic complexity, and neural networks between animals and humans.[1–3] There is, therefore, a need for a reliable model of living human neural tissues amenable to functional network assessment.

Human neural tissues with 3D cytoarchitectures have been engineered from human pluripotent stem cells (hPSCs), including induced pluripotent stem cells (iPSCs) and human embryonic stem cells (hESCs), using culture systems like hydrogel cultures,[4,5] scaffold-based cultures,[6,7] acoustic levitational assembly,[8] self-organized brain spheroid/organoid,[9,10] and brain-on-a-chip models.[11,12] The 3D bioprinting represents more precisely controlled and defined technology for fabricating human neural tissues by spatial deposition of living cells and hydrogels into a biologically complex cytoarchitecture.[13,14] However, printing soft tissues like the brain structure is difficult due to the inability of soft biomaterials to support a complex 3D structure or of stiff gels to enable function. Although a scaffold provides a supporting structure for printing neural tissues,[15–17] it is not bona fide 3D bioprinting or cellular bioprinting via direct deposition of live cells together with the bioink. In these cultures, the scaffold or mold is first fabricated by 3D printing, and then, the cells are seeded on the scaffold or mold. Neural cells in the scaffold or mold were not evenly distributed and formed large and thick aggregates or cell clusters.[15,17] More importantly, the scaffolds and molds are not biodegradable and block neural cell migration and, in particular, neural network formation between layers. The 3D bioprinted neural tissues that are fabricated using soft gel, such as gellan gum,[18] alginate,[19] or gelatin mixed with fibrin,[20] and printed layer by layer vertically exhibit layered structures with a certain degree of neuronal maturation. However, printed human neural tissues with functional neuron-neuron or neuron-glial connectivity within or between tissue layers were not shown (Table S1).

Here, we present a technology platform for assembling neuronal and glial subtypes into defined 3D neural tissues in which neurons and glia form functional connections within and between tissue layers using extrusion bioprinting. This is achieved by printing one layer or band next to another horizontally rather than the traditional way of stacking the layers vertically. These specially designed 3D neural tissues can be maintained by the conventional culture systems and are amenable to easy live-cell imaging and electrophysiological recording, providing a new platform for examining human neural networks under physiological and pathological conditions.

DESIGN

Our goal is to construct a layered neural tissue in which neural progenitor cells (NPCs) mature and form synapses within and across layers, while the structure is maintained. The biomaterial for tissue printing, or bioink, is the key for the success of bioprinting. The properties of this bioink need to (1) support the survival of printed cells, (2) promote the functional maturation of neural cells, (3) sustain designed cell distribution, (4) possess adjustable gelation time, and (5) maintain the structural stability of the gel. The fibrin hydrogel, consisting primarily of fibrinogen and thrombin, has been shown to be biocompatible for neural cells.[8,20,21] Thus, we choose fibrin gel as the basic bioink in our printing process.

The bioprinting strategies include droplet-based, extrusion-based, and laser-based methods. The extrusion 3D bioprinting deposits gel layer by layer and can be utilized to mimic the brain structure, such as the laminations of the human cortex. Fabrication of multi-layered brain tissues is typically performed by stacking layers or assembling layers vertically.[18,19,22] Construction of such kind of tissues requires the support with stiff gels, which, however, inhibit the growth of neurites (nerves) and, in particular, the functional connections (e.g., synapses) between neural cells.[23,24] The dimension of the printed tissue is another key factor in designing the 3D bioprinting. The diffusion limit of oxygen is limited to roughly 100–200 μm for avascular tissues.[25] The ''thick'' neural tissues limit the transfer of oxygen and nutrients, impairing the growth and function of the printed neural cells without the vascular system. Thus, the ideal thickness of the printed brain tissue would be around 100–200 μm. Further considerations in the design included the ease of morphological and functional assays as well as broad application in ordinary laboratories. We hence chose a thickness of 50 μm for each layer. In addition, unlike the traditional ways of stacking the tissue layers vertically,[18] we constructed a multi-layered tissue by depositing the layers horizontally next to each other. Together, this design enabled the construction of a relatively thin but multi-layered and functional neural tissue with defined cellular compositions and desired dimensions, which can be maintained and assayed with ease in an ordinary laboratory.

RESULTS

Developing bioink for printing human neural tissues

We first identified an optimal concentration of fibrinogen and thrombin by measuring the survival of hPSC-derived cortical NPCs (Figures 1A–1C and S1A–S1F). The cell viability decreased with the increasing thrombin concentrations at the fixed fibrinogen concentration of 2.5 mg/mL, whereas it was not influenced by the increasing concentrations of fibrinogen at the fixed low concentration of thrombin (0.5 U) (Figures S1E and S1F). The cells, however, tended to aggregate at higher fibrinogen levels (data not shown). We hence chose 2.5 or 5 mg/mL fibrinogen with 0.5 or 1 U thrombin for identifying an optimal gelation time.

We then assessed the optimal gelation time. At a constant concentration of fibrinogen (5 or 2.5 mg/mL), the gelation time decreased with the increased level of thrombin (Figure S1C). At 0.5 U thrombin, the gelation time also reduced with increasing fibrinogen concentrations (Figure S1C). We chose 2.5 mg/mL fibrinogen and 0.5 U thrombin for hydrogel construction, yielding a gelation time of about 145 ± 10 s (Figure S1C), which would be sufficient for printing a 24-well plate. Under this condition, more than 85% of the cells survived after 6 h of culturing in the fibrin gel and about 80% of the cells remained viable for 7 days (Figures 1B and 1C). We, therefore, used this composition of fibrin gel for the following experiments.

The fibrin gel itself has a low printability due to its high viscosity. We combined fibrin gel with other hydrogels that are commonly used for printing,[26–29] including gelatin, alginate, Matrigel, hyaluronic acid, and nanofibrillated cellulose (Table S2). Matrigel and hyaluronic acid presented high cell viability rates of 92.19% ± 4.26% and 85.13% ± 6.05%, respectively, although Matrigel frequently clogged the nozzle (Figure S1D; Table S2). Thus, we developed a printable bioink based on fibrin gel mixed with hyaluronic acid for our neural tissue printing.

A special requirement for neural tissue printing is that the bioink must support neurite growth and synaptogenesis. The cortical NPCs, differentiated from GFP- or mCherry-labeled hESCs for 21 days, expressed forebrain cortical progenitor markers FOXG1 and PAX6 (Figures S1A and S2B). When cultured in the fibrin gel, the progenitors became process-bearing (Figures 1D and S1G) TUJ1$^+$ neurons (Figure S1H) at as early as day 4 after printing and progressively expressed mature neuronal markers MAP2 and NeuN (Figure 1E). Many neurons displayed a pyramidal morphology after 1 month of culture in the gel (Figures 1E and 1F). Importantly, the neurons extended elaborate neurites with fine dendritic structures revealed by GFP labeling (Figure 1D). This was confirmed by positive staining for drebrin, a dendritic spine marker at day 40 (Figure 1G). Synaptic puncta, identified by staining for vGlut1 and synapsin (SYN1), were observed on TUJ1 or MAP2 neurites at day 35 (Figures 1H, 1I, and S1I). Collectively, the fibrin gel supports the maturation and synaptogenesis of the cortical neurons.

Printed neural cells mature and retain the tissue structure

A basic requirement for printing functional neural tissues is to enable neuronal maturation while maintaining the tissue structure. We printed the cell layer, or ''band'' of ~50 μm thickness, horizontally one after another. These horizontal ''bands,'' when turned 90°, exhibit vertical ''layers'' (Figure 2A). To better visualize our printed tissue construct, the GFP- or mCherry-labeled NPCs were loaded in the bioink and printed one band at a time at the dimension of 5,000 (L) × 500 (W) × 50 (H) μm (Figure 2A; Video S1). To prevent the mix of the printed bands, we added the crosslinking agent thrombin immediately following the deposit of

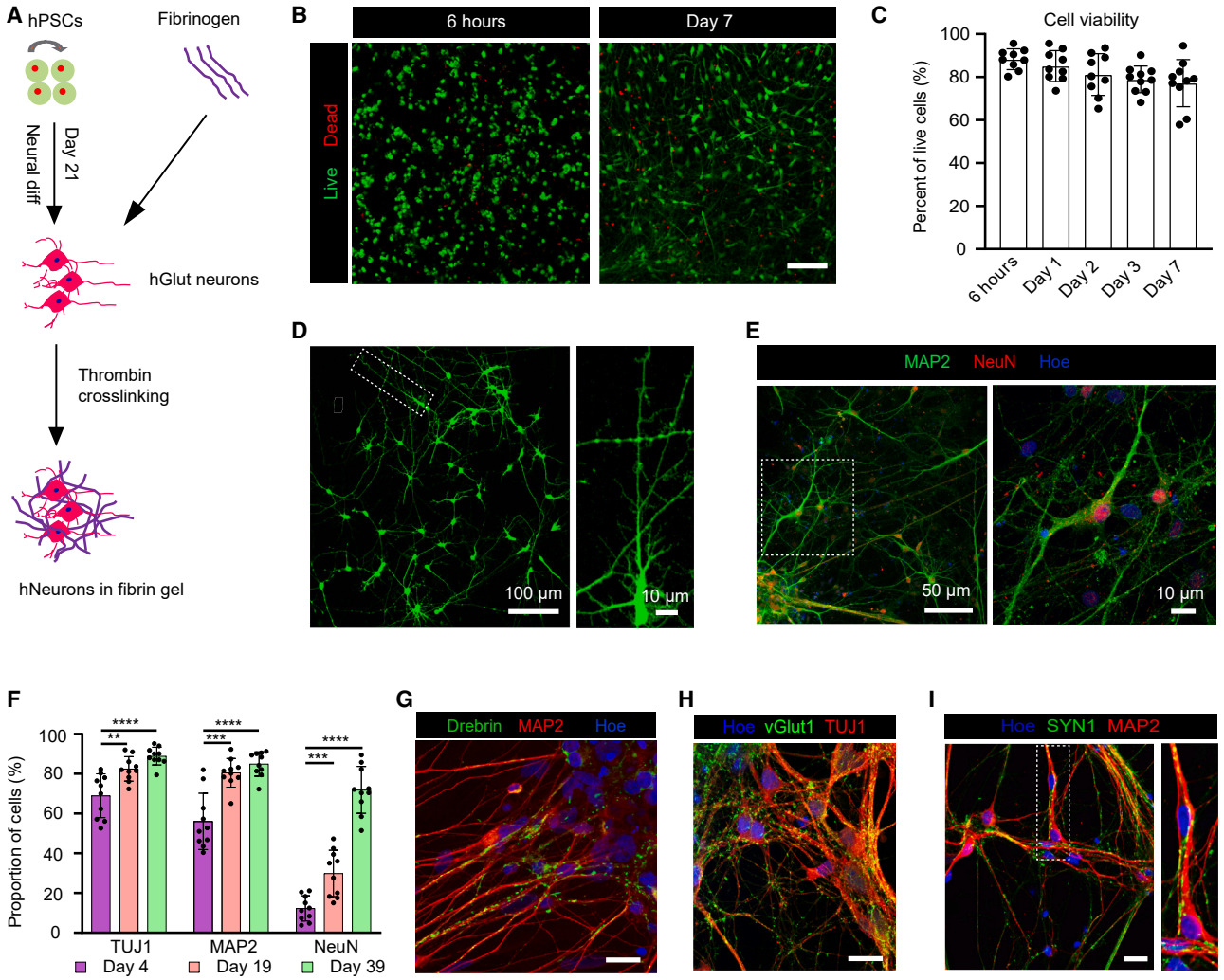

Figure 1. Survival and differentiation of hPSC-derived neurons in fibrin hydrogel

(A) Schematic diagram illustrating the growth of hPSC-derived NPCs in fibrin gel. hPSCs, human pluripotent stem cells; diff, differentiation; NPCs, neural progenitor cells; hGlut neurons, human cortical glutamatergic neurons. hNeurons, human neurons.

(B) Live and dead staining (green: "live" and red: "dead") of neural cells grown in fibrin gel at 6 h and day 7.

(C) Viability (percentage of live cells) of neural cells at different time points (n = 9–10 from at least three different experiments).

(D) Neurons showed a pyramidal morphology and formed dendritic spine-like structures, revealed by GFP after 1 month of growth in the gel.

(E) Immunostaining for neuronal markers MAP2 and NeuN at day 39.

(F) Quantitative analysis of the expression of TUJ1, MAP2, and NeuN for days 4, 19, and 39 in the fibrin gel. (n = 10 from at least three experiments. TUJ1, days 4 vs. 19, multiple t test, ** $p < 0.01$; days 4 vs. 39, multiple t test, **** $p < 0.0001$. MAP2, days 4 vs. 19, multiple t test, *** $p < 0.001$; days 4 vs. 39, multiple t test, **** $p < 0.0001$. NeuN, days 4 vs. 19, multiple t test, *** $p < 0.001$; days 4 vs. 39, multiple t test, **** $p < 0.0001$.).

(G) Immunostaining for dendritic spine marker drebrin with MAP2 at day 43 in the gel.

(H and I) Immunostaining for synaptic markers vGlut1, SYN1 with TUJ1, or MAP2 at day 35 in the fibrin gel.

Data are represented as mean ± SEM. Hoe, Hoechst 33342. Scale bars, 200 µm (B), 20 µm (G and H), and 10 µm (I). See also Figure S1.

the cell-gel mixture to form the desired shape before printing the next band (Figure 2A; shape design based on the Data S1 files). The printed neural tissue constructs were generated with multi-layered patterns (Figures 2B and S1J). Indeed, the GFP^+ cells in one band were well separated from the $mCherry^+$ cells in the next while becoming $MAP2^+$ maturing neurons at 7 days after printing (Figure 2C). Although the printed cells stayed within the designated areas, the neurons extended processes in and across the bands (Figures 2D and S1K). There were multiple cell layers in depth of the 50 µm-thick tissues (Figure 2D; Video S2), which were maintained by the conventional culture system and monitored by conventional microscopy. Thus, the printed tissue retains a stable structure within which the neural progenitors mature and form neural networks.

Neuronal subtypes form functional networks in printed tissues

The brain functions through interactions between different neuronal types. In the cerebral cortex, two major neuronal types, GABAergic interneurons and glutamatergic neurons, synapse

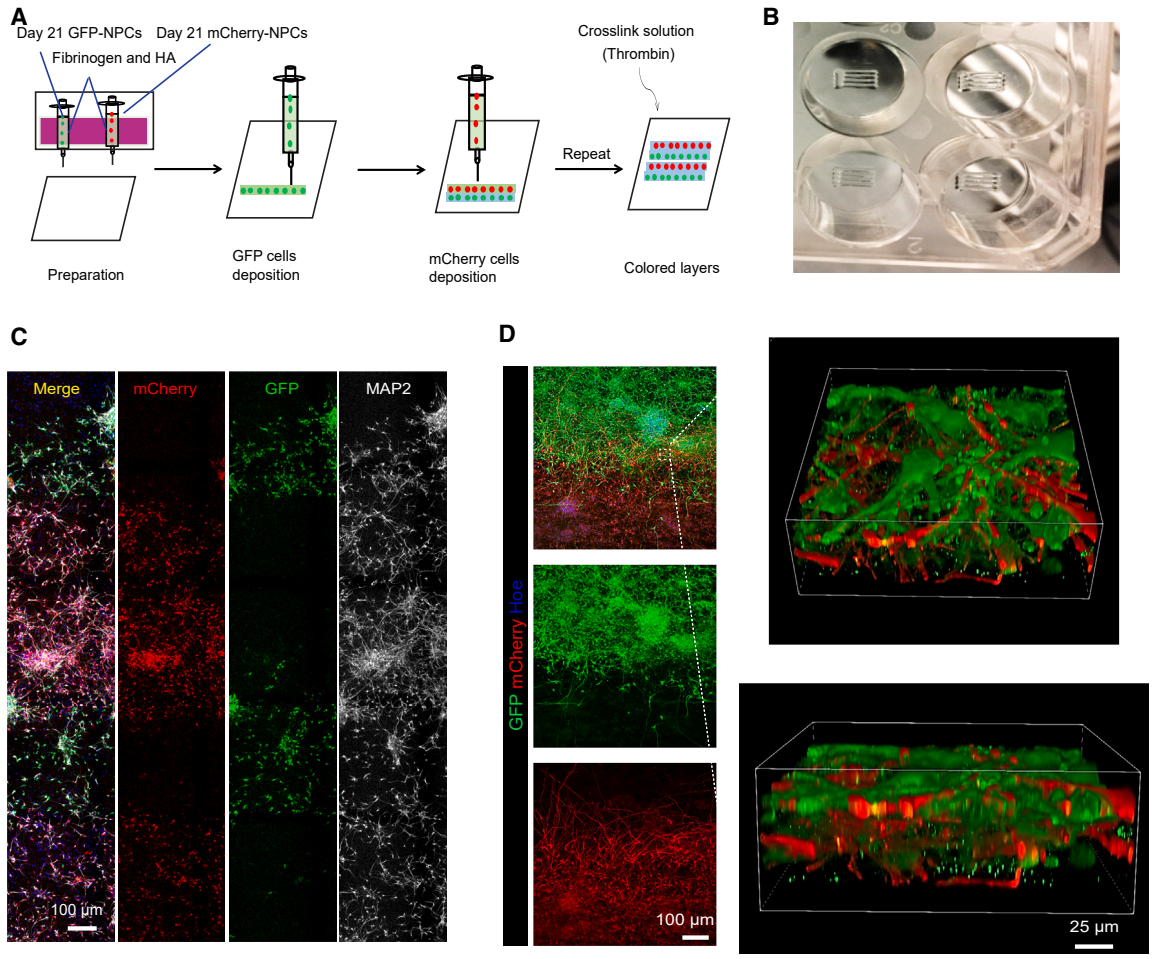

Figure 2. Printing neural tissues by design

(A) Design of the printing process for layer-patterned neural tissues. Video S1 shows the printing process. HA, hyaluronic acid.

(B) Overview of the printed structure (5,000 × 500 × 50 μm) using the testing bioink in a 24-well plate.

(C) Printed neural tissue with the "green-red-green-red" layered pattern 7 days post-printing immunostained for MAP2.

(D) Printed neural tissue with a "green-red" layered pattern (15 days post-printing), immunostained for GFP and mCherry. The inset is enlarged with a 3D reconstruction view. Video S2 shows 3D reconstruction of printed neurons.

Blue color, Hoechst 33342 staining. Hoe, Hoechst 33342. See also Figure S1 and Table S2.

and interact with each other. To determine whether these two neurons form synaptic connections when incorporated into the printed tissues, we generated medial ganglionic eminence (MGE)-derived Gamma-aminobutyric acid (GABA) and cortical (glutamate) progenitors from GFP$^+$ and GFP$^-$ hPSCs and mixed the two progenitor populations at a ratio of 1:4 before printing to mimic the ratio of interneurons to cortical projection neurons in the cerebral cortex[30,31] (Figure 3A). The hPSC-derived MGE cells at day 21 expressed NKX2.1 and GABA and were negative for PAX6 (Figures S2A–S2C), whereas the cortical progenitors were positive for PAX6 and FOXG1 (Figure S1A). To show the maintenance of the layered structure while examining the neuronal connections within and between the bands, we printed a two-layered tissue in which one band was GFP$^+$ cells and the other was non-colored cells, and each band contained the same proportion of interneurons and cortical projection neurons (Figure 3A). The printed tissue with only cortical projection neurons was served as a reference. As shown in Figure 3B, both the GFP$^+$ and GFP$^-$ bands displayed an even distribution of GABA$^+$ neurons and all MAP2$^+$ neurons. The GABA$^+$ cells comprised about 20% of the total MAP2$^+$ neuronal population at day 3 post-printing, and this ratio was maintained at day 20 (Figures 3C, 3D, S2D, and S2F). As a reference, a few GABA$^+$ interneurons (less than 1.5%) were found in the tissue printed with cortical progenitors only (Figures S2E and S2F). Hence, the neuronal subtypes in the printed tissue were maintained over time.

Examination of the tissues printed from the non-colored hPSCs (Figure S3A) at a longer time post-printing (day 60) indicated that the cortical neurons expressed cortical transcription factors TBR1, CTIP2, and SATB2 (Figure S3B). We also observed GABAergic subtypes, labeled by calretinin (CR), calbindin (CB), parvalbumin (PV), and somatostatin (SST) (Figure S3C). Therefore, the printed neural tissue constructs support

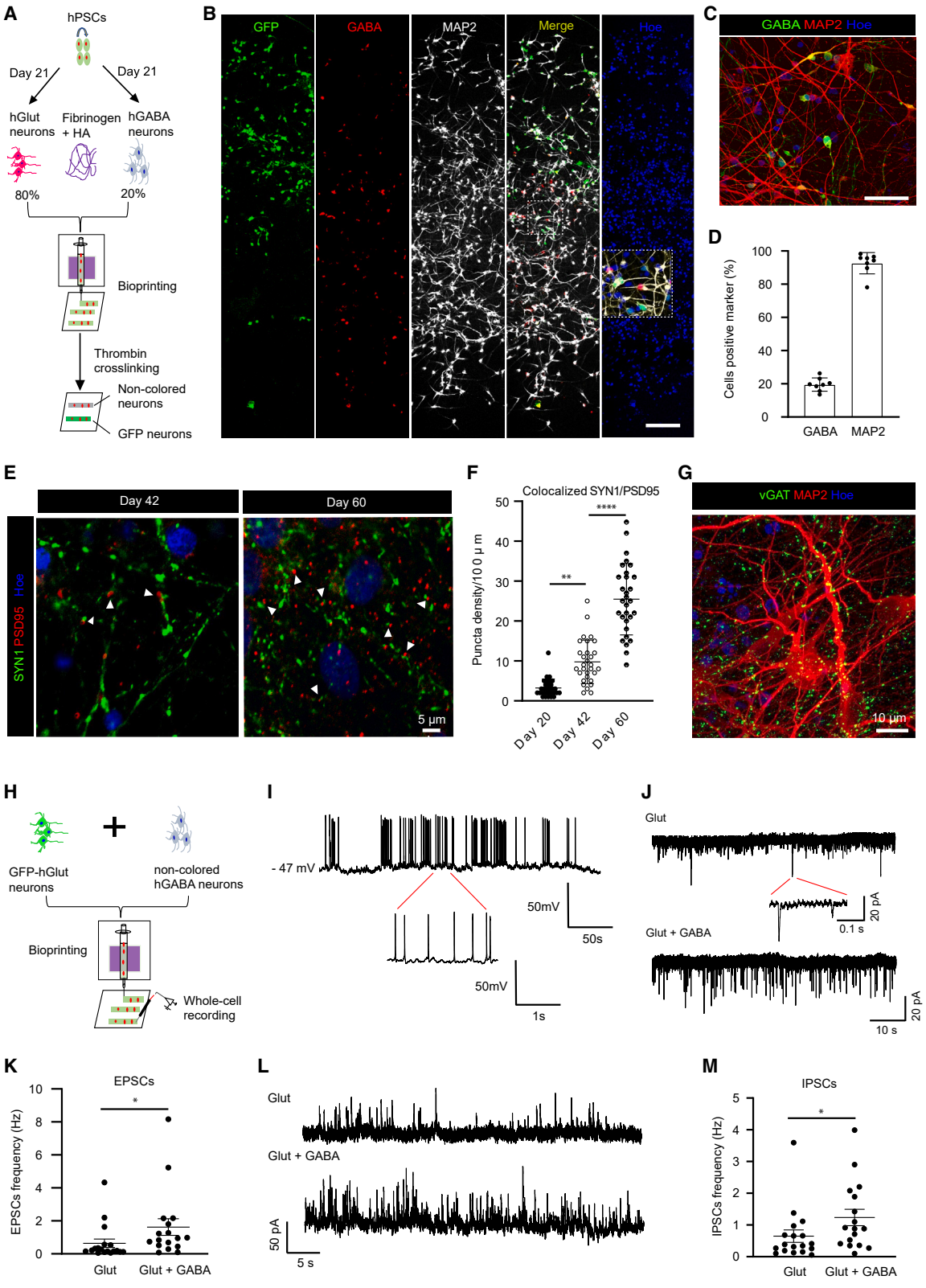

Figure 3. Functional connections between neurons in the printed tissue

(A) Schematic diagram illustrating the design of experiments.

(B) Immunostaining of the tissue for GABA and MAP2 (3 days post-printing; scale bars, 100 μm).

(legend continued on next page)

the maturation of cortical glutamatergic neurons and GABAergic interneurons.

Neuronal maturation was reported in printed 3D human neural tissues showing expressions of MAP2 and NeuN (Table S1). We found the co-expression of the pre- and postsynaptic markers, SYN1 and PSD95, as early as day 20 after printing (Figure 3E), indicating the formation of synapses, which usually needs longer time to form in 2D cultures.[32,33] The synaptic puncta density increased over extended culture (Figures 3E and 3F). More SYN1 puncta density was present in the printed tissues with both glutamate and GABA neurons than in prints with only glutamatergic neurons (Figures S3D and S3E), suggesting that the interactions between glutamatergic neurons and GABAergic neurons promote synaptogenesis. The GABAergic neurons also formed synapses as indicated by the expression of inhibitory presynaptic protein vGAT (Figure 3G). Furthermore, the excitatory presynaptic marker vGlut1 and inhibitory postsynaptic marker gephyrin were expressed at day 25 after printing, and more vGlut1 and gephyrin puncta were observed at day 45 (Figure S3F). These observations indicate the formation of excitatory and inhibitory synapses in the printed neural tissues.

The most challenging aspect of human neural tissue printing is the formation of functional networks. To date, few 3D-printed human neural tissues show functional connectivity except for cells seeded in the pre-set scaffolds or molds (Table S1). Given the appropriate thickness of the printed tissue construct, we performed electrophysiological recording of the tissues that were printed with GFP^+ glutamatergic cortical progenitors and non-colored MGE GABAergic progenitors (Figure 3H). Whole-cell patch clamping indicated that the glutamatergic neurons exhibited inward Na^+ and outward K^+ currents (Figures S4A–S4C) and evoked action potentials (eAPs) about 3 weeks after printing (Figure S4D); these neurons also exhibited spontaneous action potentials (sAPs) (Figure 3I). The percentage of cortical neurons with sAPs increased over time, particularly in the prints with the incorporation of GABAergic neurons (36.36% vs. 47.06% for 3 weeks and 50% vs. 71.43% for 5 weeks) (Figure S4E). The frequency of sAPs also increased with time, and printed tissues with GABAergic and glutamatergic neurons showed more sAPs (Figures S4F and S4G), suggesting functional maturation of the printed neurons. Importantly, the glutamatergic neurons displayed excitatory and inhibitory postsynaptic currents (EPSCs and IPSCs), suggesting the formation of functional networks between glutamatergic neurons and GABAergic interneurons (Figures 3J and 3L). Moreover, these cells received more EPSCs and IPSCs when printing together with GABAergic neurons (Figures 3K and 3M). The hPSC-derived cortical GABAergic interneurons usually mature very slowly.[34] In the printed tissue, the GABAergic interneurons generated sAPs at day 21 (Figure S4H). Spontaneous IPSCs were observed in the GABA neurons at day 35, and the IPSCs were abolished by the $GABA_A$ receptor antagonist bicuculline (Figure S4I), indicating that GABA neurons were also functionally mature. These results confirm the functional maturation of cortical projection neurons and GABAergic interneurons and the functional connection among neurons within the printed tissues.

Neurons and astrocytes form functional networks in printed tissues

Appropriate neuronal network function requires the presence of glia, including astrocytes. We hence incorporated hPSC-derived astrocyte progenitors (Figures S5A and S5B) into the above glutamate neurons and GABA interneurons at a ratio of 4:5:1 within the printed tissue. We also printed a two-layered tissue consisting of GFP^+ and GFP^- cells, and each band had three cell types (Figure 4A). The glial fibrillary acidic protein-positive ($GFAP^+$) astrocytes and the $MAP2^+$ neurons were distributed throughout the printed tissue (Figure 4B), as were $GABA^+$ interneurons (Figure S5C). Quantitative analysis of GABA, MAP2, and GFAP expressions showed that the proportion of the three cell types in printed neural tissues was maintained (Figure S5E).

In the prints with both neurons and astrocytes, most of the neurons (>90%) became $NeuN^+$ neurons at day 30 post-printing (Figures S6D and S6E). Particularly, we discovered that astrocytes became progressively more mature over time, with more elaborate processes and branches (Figures 4C, 4D, S6B, and S6C). While GFAP staining showed extensive branches of astrocyte processes (Figure 4D), GFP labeling revealed fine processes and their sheets (Figures 4F, S6I, and S6J). Notably, 3D visualization showed that the astrocytic branches were intertwined with the mCherry-neuronal processes (Figures 4G and S6J), suggesting close neuron-astrocyte interactions.

Astrocytes, in response to neuronal stimulation, generate calcium signals; this enables them to modulate neuronal

(C) Immunostaining of tissues for GABA and MAP2 (20 days post-printing; scale bars, 50 μm).
(D) Quantitative analysis of GABA and MAP2 cell populations (8 samples from three different batches were analyzed).
(E) Immunostaining for synaptic markers SYN1 and PSD95 at days 42 and 60. White triangles indicate the co-localized puncta of SYN1 and PSD95.
(F) Quantitative analysis of co-localized SYN1 and PSD95 puncta density over time (one-way ANOVA, $^{**}p < 0.01$, $^{****}p < 0.0001$, 30 neurons from three different experiments were analyzed).
(G) Immunostaining for synaptic markers vGAT with MAP2 at day 30.
(H) Schematic diagram illustrating the electrophysiological recording of printed tissues.
(I) Spontaneous action potentials (sAPs) of glutamate cortical cells from printed tissues incorporated with Glut and GABA neurons at day 21 post-printing.
(J) Representative traces of EPSCs recorded from glutamatergic neurons in tissues with Glut neuron-only or Glut and GABA (Glut + GABA) tissues at 5 weeks post-printing.
(K) Quantitative analysis of EPSC frequency for different groups 5 weeks after printing (Mann-Whitney U test, $^{*}p < 0.05$; 18 neurons from five different batches were analyzed for Glut condition and 17 neurons from five different batches were analyzed for Glut + GABA condition).
(L) Representative traces of IPSCs recorded from glutamatergic neurons in printed tissues with Glut neuron-only or Glut and GABA neurons (Glut + GABA) at 5 weeks post-printing.
(M) Quantitative analysis of IPSC frequency for different groups 5 weeks after printing (Mann-Whitney U test, $^{*}p < 0.05$; 18 neurons from five different batches were analyzed for the Glut group and 17 neurons from five different batches were analyzed for the Glut + GABA group).
Data are represented as mean ± SEM. Hoe, Hoechst 33342. See also Figures S2–S4.

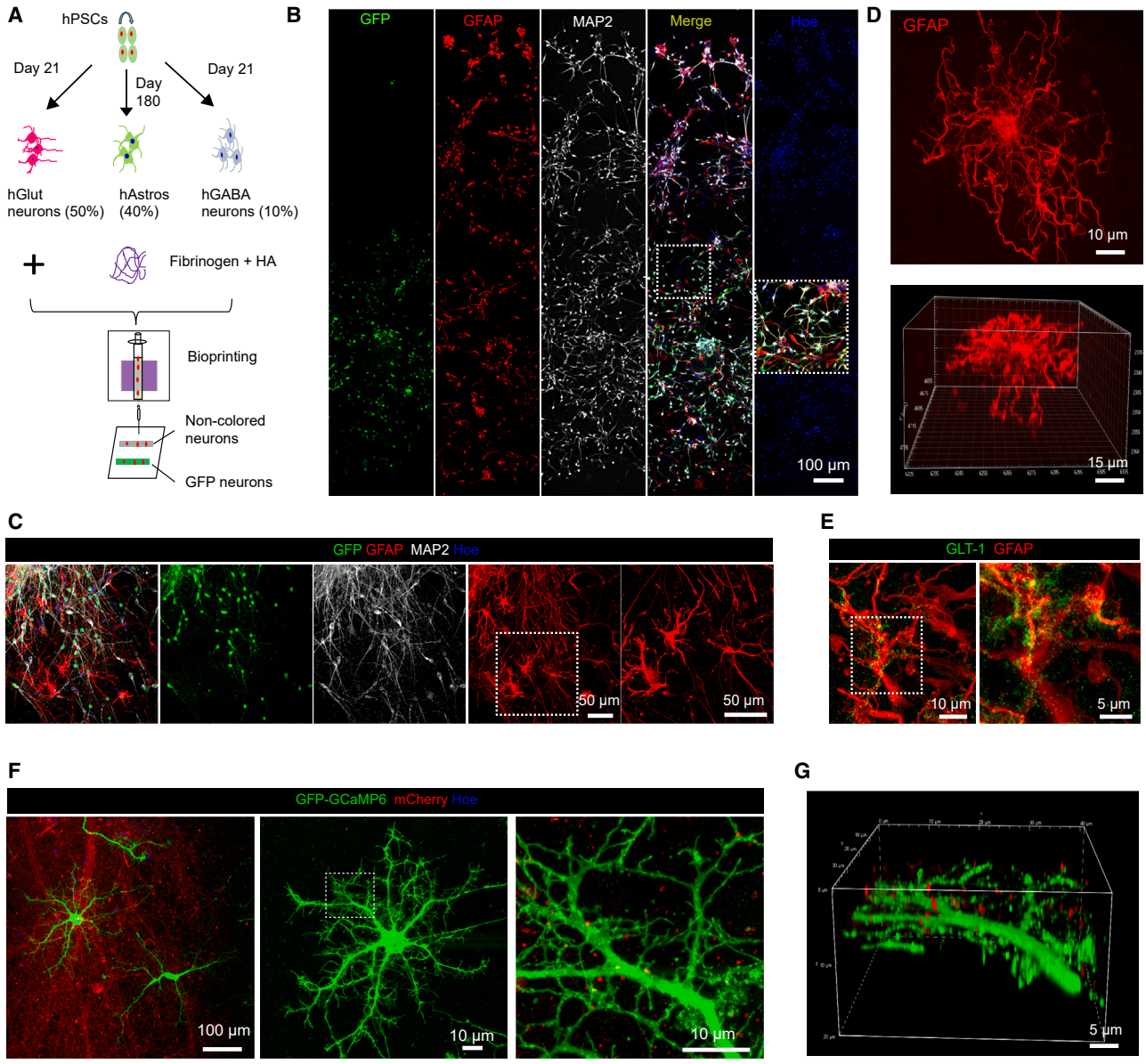

Figure 4. Incorporation of astrocytes with neurons in printed tissues

(A) Schematic diagram illustrating the design of experiments.

(B) Immunostaining of the tissue for GFAP and MAP2 (3 days post-printing). Hoe, Hoechst 33342.

(C) Immunostaining of astrocytes and neurons in printed tissues for GFAP and MAP2 at day 60 post-printing. Hoe, Hoechst 33342.

(D) The 3D morphology of astrocytes with staining of GFAP in printed tissues at day 60.

(E) Immunostaining of tissues for GLT-1 and GFAP at day 40.

(F) Immunostaining for GFP-GCaMP6 and mCherry at day 30 post-printing.

(G) 3D imaging from (F).

See also Figures S5 and S6.

networks.[35,36] Neurons and astrocytes were printed together into neural tissues[17,37,38] (Table S1), but whether they form functional connections is not known. To determine whether the astrocytes functionally integrate into the printed neural networks, we printed mCherry-labeled neurons with lentivirus-GCaMP6-infected astrocytes (Figure 5A). We found that the application of a high-concentration KCl solution, which depolarizes neurons but does not obviously affect astrocytes directly, elicited calcium responses in astrocytes in the printed tissues (Figures 5B and 5C). The total $\Delta F/F$ of GCaMP6 signals increased from 2 to 6 weeks after printing (Figure 5D). Thus, the neurons and astrocytes in the printed tissues are functionally connected.

One of the most important functions of astrocytes is to recycle neurotransmitters like glutamate that are released to the

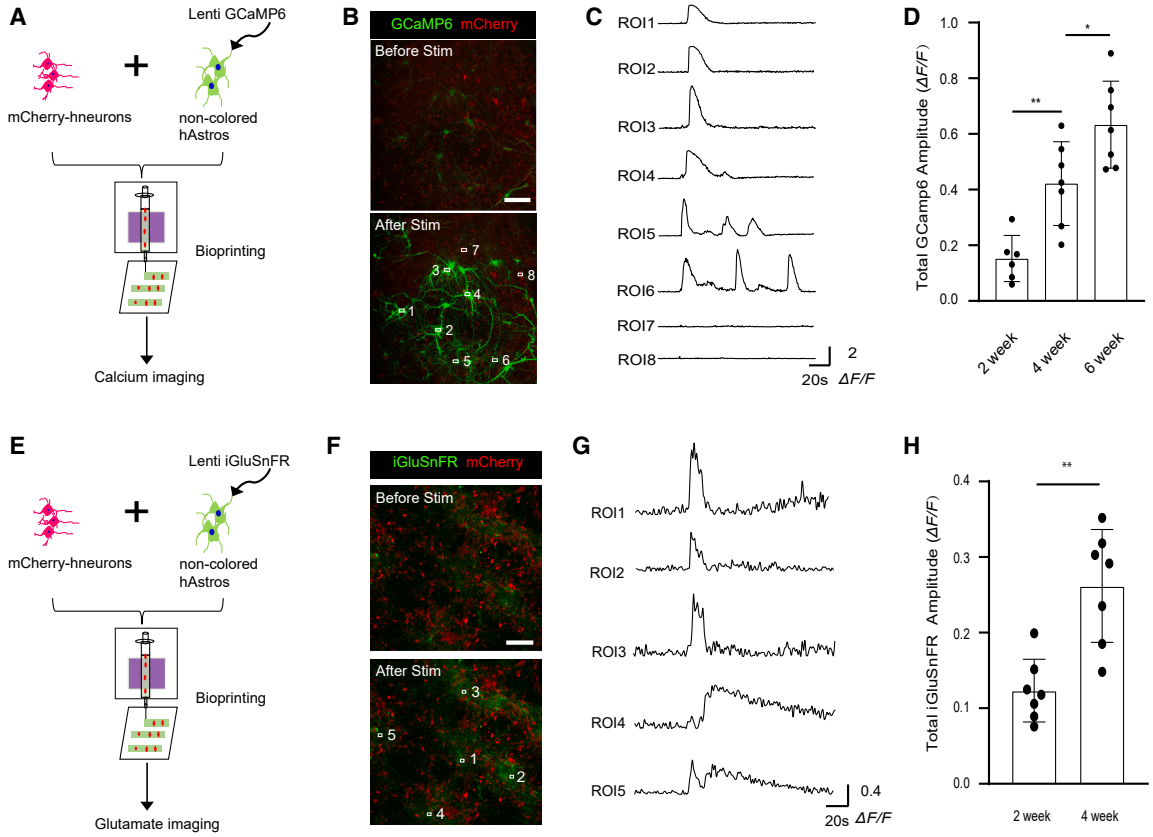

Figure 5. Neural network between neurons and astrocytes in the printed tissue

(A) Schematic diagram illustrating calcium imaging of printed tissues with neurons and astrocytes. Neurons were mCherry labeled, and astrocytes were infected with lentivirus-GCaMP6 before printing.

(B) Cells in printed tissues responding to neuronal stimulation with a high concentration of KCl solution (scale bars, 100 μm).

(C) Representative traces of GCaMP6 imaging. ROIs 1–6 indicate GCaMP6-astrocytes and ROIs 7 and 8 indicate mCherry-neurons. ROI, region of interest.

(D) Total GCaMP6 amplitudes of $\Delta F/F$ in tissues at 2, 4, and 6 weeks after printing (one-way ANOVA, $^{**}p < 0.01$; $^{*}p < 0.05$, 6–7 samples from 3 different batches were analyzed for each time point).

(E) Schematic diagram illustrating glutamate imaging of printed tissues with neurons and astrocytes. Neurons are mCherry labeled, and astrocytes were infected with lentivirus-iGluSnFR before printing.

(F) Cells in printed tissues responding to neuronal stimulation with a high-concentration KCl solution (scale bars, 100 μm).

(G) Representative traces of iGluSnFR imaging. ROIs 1–5 indicate iGluSnFR-astrocytes.

(H) Total iGluSnFR amplitudes of $\Delta F/F$ in tissues at 2 and 4 weeks after printing (t test, $^{**}p < 0.01$, 7 samples from three different batches for each time point). Data are represented as mean ± SEM.

synaptic cleft.[36] Indeed, the astrocytes expressed glutamate transporter 1 (GLT-1) at day 40 post-printing (Figure 4E), suggesting the maturation of astrocytes. We further examined networks between neurons and astrocytes using live imaging of a glutamate indicator iGluSnFR (Figure 5E). Again, when we applied KCl solution, which triggers cortical neurons to release glutamate but does not have an obvious effect on astrocyte-only cultures, the iGluSnFR signals in astrocytes were induced (Figures 5F and 5G). The total $\Delta F/F$ of iGluSnFR signals increased from 2 to 4 weeks after printing (Figure 5H). Therefore, astrocytes can take up glutamate released from neurons in the printed tissues.

Functional networks form between the printed cortical-striatal tissue layers

Neurons not only synapse with each other in the same brain region but also connect to each other between nuclei or layers. Neural tissues printed in a thick stack do not project neurites (nerves) across the layers (Table S1). To assess the functional connectivity between tissue layers, we printed cortical neurons with DARPP32^{+} striatal medium spiny neurons (Figure 6A). The striatal neurons showed high expressions of GABA and DARPP32 (Figures S7A–S7D). After printing, cortical neurons expressed GFP; and striatal neurons, expressing mCherry and DARPP32, showed a distinguished tissue separation (Figure S7E). Both neuronal types became mature with the expression of MAP2 at 2 weeks after printing (Figure S7F). The printed cortical and striatal neuronal bands were well maintained 15 days after printing, and GFP and mCherry neurites grew toward each other although the GFP-labeled cortical neurites projected deeper into the mCherry-labeled striatal band (Figure 6B). The projected cortical neurites (axons) formed physical contacts with the striatal neurites (Figure S7G; Video S3), indicating the formation of a connection.

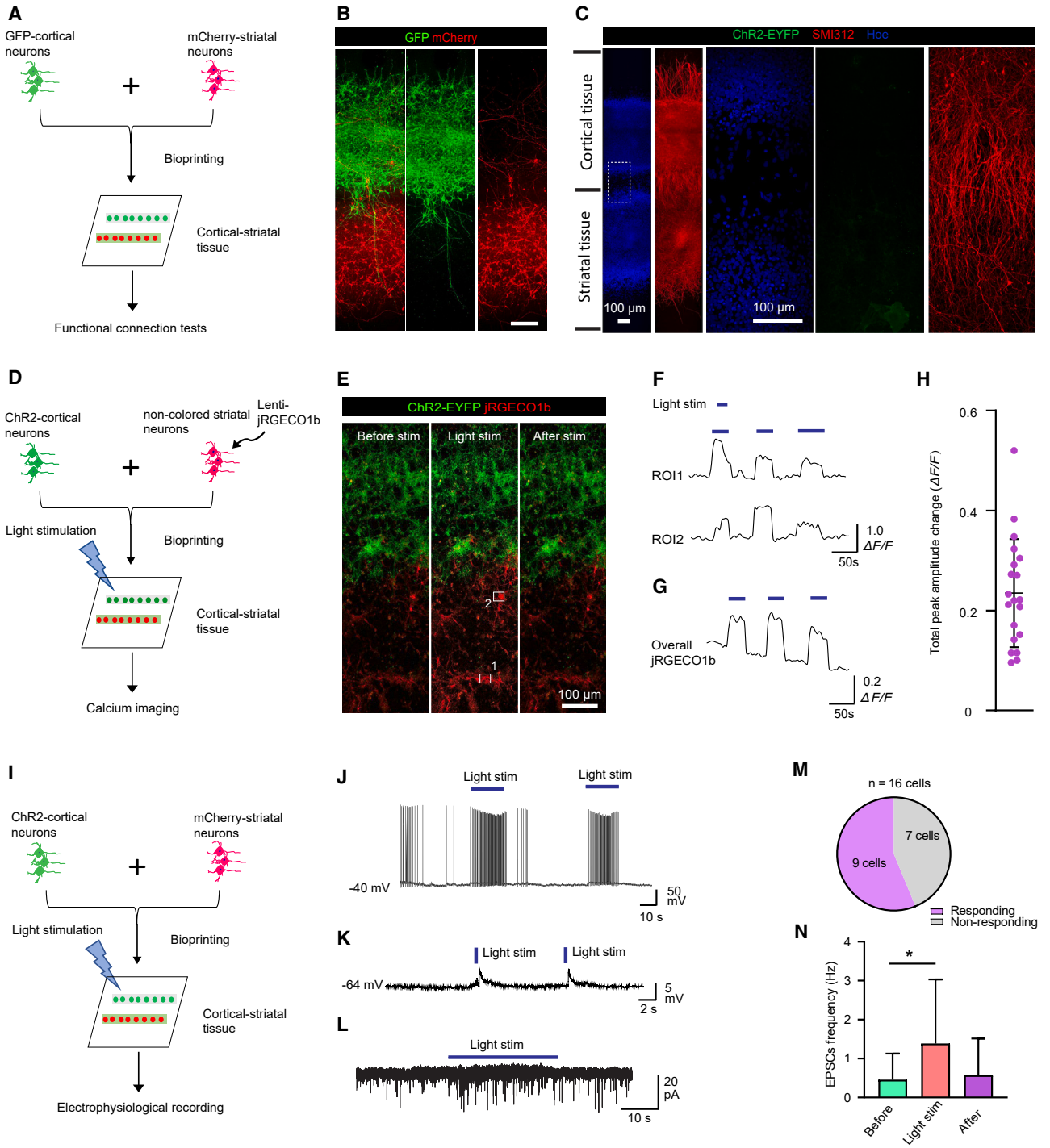

Figure 6. Functional network between cortical and striatal neuronal layers

(A) Schematic diagram illustrating the design of experiments for printing the cortical-striatal tissue.

(B) Immunostaining of the tissue for GFP and mCherry to show the printed cortical-striatal layers at 15 days post-printing (scale bars, 100 μm).

(C) Immunostaining of cells for the axonal marker SMI312 in the 3D printed tissue (4 weeks after printing).

(D) Schematic diagram illustrating calcium imaging of printed tissues with cortical and striatal neurons. Cortical neurons expressed ChR2, and striatal neurons were non-colored and infected with lentivirus-jRGECO1b before printing.

(E) Printed tissue (2 weeks post-printing) responding to light stimulation, showing changes in jRGECO1b signals (red) before and after stimulation.

(F) Representative traces of calcium imaging from two ROIs. ROI, region of interest.

(G) Total traces of calcium imaging.

(H) Total jRGECO1b amplitudes of $\Delta F/F$ in tissues after light stimulation (21 samples from five different batches).

(legend continued on next page)

In the brain, cortical neurons (deep layers) project axons to the striatum. In our print, we observed neurites growing toward each other (Figure 6B). To determine whether the cortical and striatal neuron axons project to each other, we performed the immunostaining of the printed tissue with an axonal marker SMI312 when the cortical-striatal tissue was printed with a gap of 100 μm between the bands (Figure 6C). Strikingly, we found that the axonal projection was from the cortical neurons to striatal neurons but not from the striatal to cortical neurons (Figure 6C). This pattern of axonal projection resembles that *in vivo* where cortical neurons project axons to the striatum, demonstrating the striking specificity of neuronal network formation in the printed tissues.

To determine whether neurons in the printed cortical tissue form functional synaptic connections with those in the striatal tissue, we printed cortical neurons that expressed Channelrhodopsin2-enhanced yellow fluorescent protein (ChR2-EYFP)[39] with striatal neurons that expressed the red calcium indicator jRGECO1b[40] (Figure 6D). We found that the application of 470-nm light to stimulate ChR2-EYFP cortical neurons elicited calcium responses in the striatal neuron band 2 weeks after printing (Figure 6E). Even the striatal neurons far from the cortical band showed increased calcium responses (Figure 6F). The total ΔF/F of calcium signals for the whole striatal neuron layer significantly increased with stimulation (Figures 6G and 6H), suggesting functional connections of the cortical neuron band with the striatal neuron band. We further characterized the functional connections between cortical and striatal neurons by patch clamping in response to light stimulation (Figures 6I, S7H, and S7I). We found that the application of 470-nm light induced burst action potentials and spontaneous excitatory postsynaptic potentials (EPSPs) in the striatal neurons 3–5 weeks after printing (Figures 6J–6L). The percentage of responsive cells for EPSCs was >56% (Figure 6M), and the frequency of EPSCs was significantly increased by light stimulation (Figures 6N and S7I). Thus, both calcium imaging and electrophysiological recording demonstrate the functional connectivity between the cortical-striatal tissue layers.

As shown above, stimulation of the ChR2-expressing cortical neurons elicited responses in the striatal neurons as assayed by calcium signaling (Figures 6D–6H). The question is whether stimulation of striatal neurons elicits responses in the cortical neurons. We printed ChR2-expressing striatal neurons and jRGECO1b-infected cortical neurons (Figure S7J). At 2 and 4 weeks after printing, light stimulation of the ChR2-expressing striatal neurons did not elicit an obvious response in the cortical neuron-based calcium imaging (Figures S7K and S7L). The lack of response from the cortical neurons to the stimulation of striatal neurons is likely due to the lack of axonal projection from the striatal neurons to cortical neurons. This finding again demonstrates the specificity of functional connections between the cortical-striatal tissues in the prints.

The printed human neural tissues are amenable to modeling pathological processes

To assess if the above printed tissues are amenable to examining pathological processes, especially at the functional level, we use Alexander disease (AxD), a neurodegenerative disease caused by mutations in the GFAP gene,[41] as an example. We assessed neuron-astrocyte interaction in the prints similar to that described in Figure 4A. In this case, the (glutamate and GABA) neurons were derived from hESCs (H9), whereas the astrocytes were derived from either AxD (R88C mutation) or isogenic control (mutation corrected by CRISPR) iPSCs[42] (Figure 7A). After printing, the AxD astrocytes displayed GFAP aggregation intracellularly in contrast to the isogenic controls (Figure 7B), which recapitulates the pathological feature of AxD.[43] The printed AxD tissues showed lower expression levels of GLT-1 than the control at day 20 post-printing (Figure 7C). By 30 days after printing, $MAP2^+$ neurons and $GFAP^+$ astrocytes displayed a complex morphology with elaborate processes and expression of synapsin (Figure 7D). Interestingly, the AxD tissues had a more significantly reduced synaptic puncta density than the tissue with isogenic astrocytes (Figures 7D and 7E), suggesting that AxD astrocytes are less supportive for synaptogenesis compared with the control astrocytes.

We have previously shown that AxD patient astrocytes in 2D cultures failed to propagate calcium waves.[42] To determine whether AxD astrocytes alter their response to neuronal function, we used the prints of normal neurons with either AxD or isogenic astrocytes infected with lentivirus-GCaMP6 (Figure 7F). Stimulating neurons with high KCl elicited a robust Ca^+ response in isogenic astrocytes. In contrast, AxD astrocytes showed significantly fewer calcium responses (Figure 7G). The total $\Delta F/F$ of GCaMP6 signals for AxD astrocytes was significantly lower over time than that of the control (Figure 7H). We further investigated the neuron-glial connections in AxD using live imaging of glutamate uptake by iGluSnFR (Figure 7I). Upon neuronal stimulation with high KCl, the AxD astrocytes in printed tissues exhibited fewer changes of iGluSnFR signals than the isogenic control (Figures 7J and 7K). At 2 and 4 weeks after printing, the total $\Delta F/F$ of iGluSnFR signals for AxD astrocytes was significantly lower than that of iGluSnFR signals for the isogenic control (Figure 7L). These results indicate that the disease-relevant functional phenotypes are readily displayed in the printed human neural tissues.

DISCUSSION

We have printed functional human neural tissues by design. We achieve it by first developing a bioink that is suitable for survival,

(I) Schematic diagram illustrating the method for whole-cell patch-clamp recording with optogenetic activation in printed cortical-striatal tissues. Cortical neurons were ChR2 cells, and striatal neurons were mCherry labeled.

(J–L) Representative electrophysiological traces of spontaneous action potentials, EPSPs and EPSCs of striatal neurons within printed tissues by light stimulation.

(M) Percentage of responsive cells with light stimulation for EPSC recording.

(N) Quantitative analysis of EPSC frequency before, during, and after light stimulation (paired t test, *$p < 0.05$; 9 neurons from three different batches).

Data are represented as mean ± SEM. Hoe, Hoechst 33342. See also Figure S7.

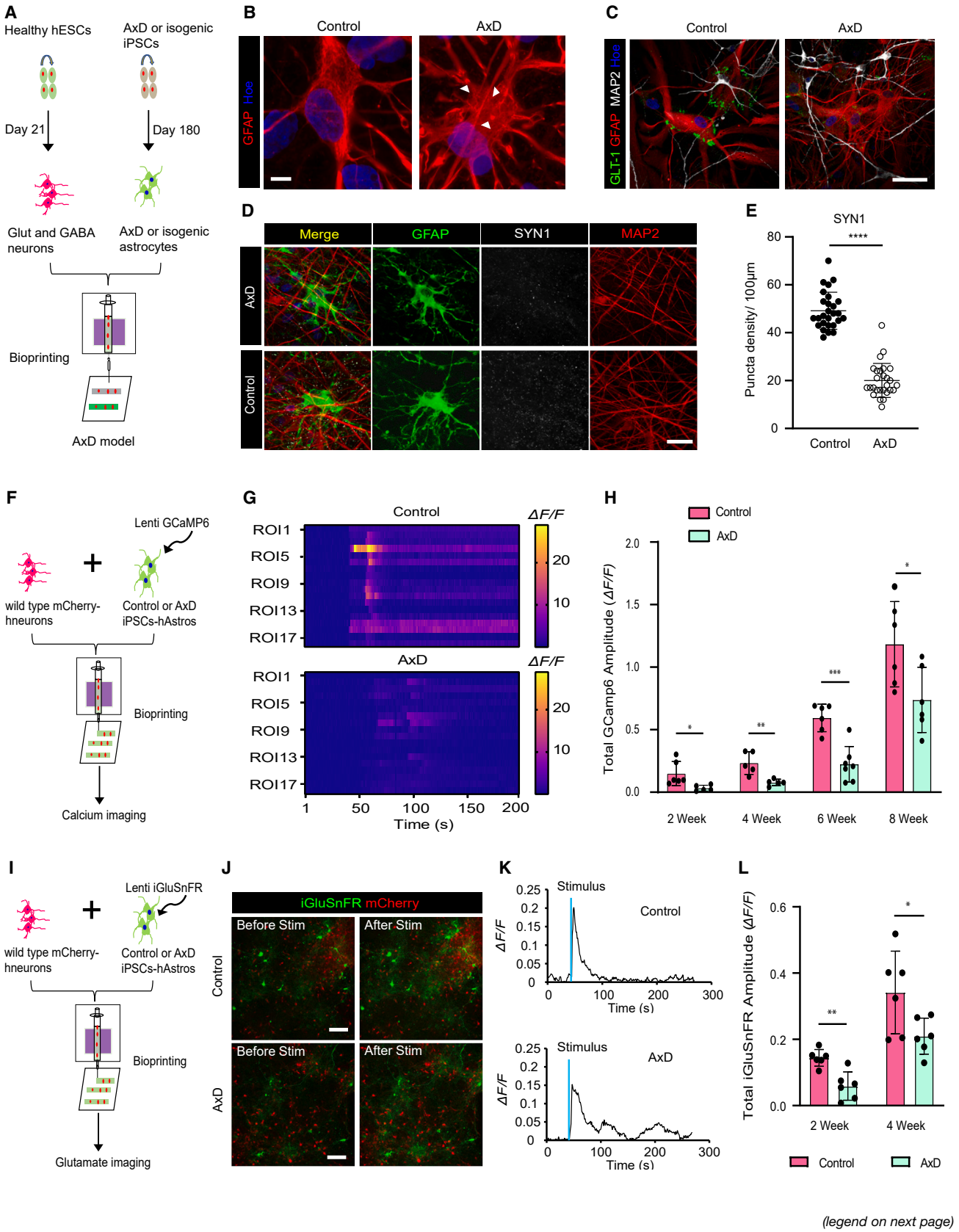

(legend on next page)

neurite growth, and synapse formation by the differentiating neurons. Then, we designed a special tissue pattern by printing the bands horizontally, allowing easy live-cell imaging and electrophysiological recording. Importantly, the printed neural tissues form functional synaptic connections between neuronal subtypes within and between tissue bands as well as functional neuron-astrocyte networks within 2–5 weeks after printing their progenitors. The brain tissues printed by design offer a defined platform for examining human neural networks under physiological and pathological conditions.

Our platform has several features. First, the functional neural circuits, indicated by EPSCs and IPSCs, are established in 2–5 weeks after printing. Multi-layered neural tissues have been fabricated through vertical deposition,[18,19,44–46] which requires stiff bioink to hold the tissue stable. These printed tissues show little functional connectivity possibly due to the stiff bioink, as only soft gels support neurite sprouting and synapse formation.[23,24] Second, the printed tissue allows the incorporation of different neuronal subtypes such as cortical glutamatergic neurons, cortical GABAergic interneurons, or striatal medium spiny neurons at defined proportions, which is difficult to achieve via organoids or other printing methods to date. Third, this platform enables the establishment of functional neuron-glial networks with a controlled neuron-to-glia ratio within 2–4 weeks, simplifying the analysis of neuron-glial interactions in the 3D environment. Fourth, functional layered tissues like the cortical-striatal tissue can be readily assembled, and the intrinsic property of tissue interaction such as axonal projection is retained, as indicated by the cortical projection to the striatal tissue. Interaction between different brain regions may also be achieved using assembloids, although the assembloids are often combined in a random fashion, and it takes much longer time for them to form functional connections.[47–49] Our tissue assembly can be printed in a defined orientation and distance and forms functional connectivity in a much shorter time. Such a printing platform provides a promising model to study human neural circuits among different brain regions. Fifth, the dimensions of the printed tissues, including the thickness, are controlled so that they allow sufficient nutrients and oxygen for the survival, growth, and function of the neural tissue under the conventional culture system. This relies on our special design of horizontal printing, overcoming thickness of the vertical printing and the spheric structure of organoids. Finally, the composition of the functional cell types depends on that of printed progenitor cells, making it predictable for the anatomical properties and potential functions of the printed tissues. Together, these features make the printed neural tissue a promising paradigm for studying human neural network functions.

Limitations

Our prototype 3D bioprinting has weaknesses. Due to the softness of the gel, our bioink does not support multiple-layer printing vertically. We also limited the thickness of the printed tissues to about 50 μm to maximize the formation of functional neural networks. Additionally, our current printing technology does not enable the orientation of the mature neurons although many neurons exhibit a pyramidal morphology. Since the tissue is assembled by design, the printed tissue lacks the intrinsic structural organization of brain organoids. Interestingly, however, some of the intrinsic properties, including the anatomical and functional neuronal connections, are retained in the printed tissue, as evidenced by the uni-directional axonal projection from the cortical tissue to the striatal tissue. On the other hand, the cells in the printed brain tissue mature rapidly and in a synchronized manner, thus complementing the existing organoids and offering a defined platform for examining human neural networks under physiological and pathological conditions. It is expected that with the advancement of bioprinting technology, more sophisticated human neural tissues may be produced with defined cellular compositions and orientation, tissue organization, and tissue assembly. Given that many neuronal subtypes can now be generated from hPSCs,[50] our platform allows printing neural tissues with a defined composition of neural types at a particular ratio, potentially enabling assessment of the biophysical nature of the human neural circuits. As exemplified by the dynamic interaction between the neuronal activation and altered response from AxD astrocytes in the printed neural tissues, the platform also provides a promising tool for studying interactions between specific neural cell types and neural circuits under pathological

Figure 7. Modeling AxD using the printed tissue

(A) Schematic diagram illustrating the design of experiments. We used a pair of AxD patient-iPSCs and its isogenic control.

(B) Immunostaining of control and AxD tissues for GFAP showing the aggregation of GFAP fibers at day 60 post-printing. White triangles indicate the GFAP aggregates. Similar results were observed in three independent experiments.

(C) Immunostaining of control and AxD tissues for GLT-1, GFAP, and MAP2 at day 20 post-printing.

(D) Immunostaining of tissues for SYN1, GFAP, and MAP2 (30 days post-printing).

(E) Quantitative analysis of SYN1 puncta density (t test, ****$p < 0.0001$, 30 samples for each condition from at three different experiments).

(F) Schematic diagram illustrating calcium imaging of printed tissues for AxD model. Healthy neurons were mCherry labeled and AxD or control astrocytes were infected with GCaMP6 before printing.

(G) Heatmap showing $\Delta F/F$ of GCaMP6 signal from control and AxD tissues.

(H) Total GCaMP6 amplitudes of $\Delta F/F$ in control and AxD tissues overtime (multiple t tests, *$p < 0.05$; **$p < 0.01$; ***$p < 0.001$, n = 6 from three different experiments).

(I) Schematic diagram illustrating glutamate imaging of printed tissues for the AxD model. Healthy neurons were mCherry labeled and AxD or control astrocytes were infected with iGluSnFR before printing.

(J) Cells in printed tissues responding to neuronal stimulation with a high-concentration KCl solution.

(K) Representative traces of iGluSnFR change ($\Delta F/F$) from the control and AxD tissues.

(L) Total iGluSnFR amplitudes of $\Delta F/F$ in the control and AxD tissues at 2 and 4 weeks after printing (multiple t tests, *$p < 0.05$; **$p < 0.01$, n = 6 from three different experiments).

Data are represented as mean ± SEM. Hoe, Hoechst 33342. Scale bars, 5 μm (B), 50 μm (C), 20 μm (D), and 100 μm (J).

conditions. The defined dimensions and cellular compositions make the platform amenable to throughput analysis and drug development.

STAR★METHODS

Detailed methods are provided in the online version of this paper and include the following:

- KEY RESOURCES TABLE
- RESOURCE AVAILABILITY
  - Lead contact
  - Materials availability
  - Data and code availability
- EXPERIMENTAL MODEL AND STUDY PARTICIPANT DETAILS
  - Human cell source
- METHOD DETAILS
  - Generation of cortical neural progenitors, GABAergic interneurons, striatal neurons, and astrocyte progenitors from hPSCs
  - Preparation of fibrin gel
  - Culturing neural cells in fibrin gel
  - Gelation testing of fibrin gel
  - Bioink preparation
  - Cell viability assay
  - Printing procedure
  - Printing neural tissues
  - Immunofluorescence and quantification
  - Synaptic puncta quantification
  - Lenti-GCaMP6 virus preparation
  - Lenti-jRGECO1b and lenti-iGluSnFR virus preparation
  - Calcium and Glutamate imaging
  - Optogenetic stimulation
  - Electrophysiology
- QUANTIFICATION AND STATISTICAL ANALYSIS

SUPPLEMENTAL INFORMATION

Supplemental information can be found online at https://doi.org/10.1016/j.stem.2023.12.009.

ACKNOWLEDGMENTS

We thank X. Chu and M. Ayala for technical assistance and K. Knobel for confocal imaging and Imaris image analysis. This study was supported in part by NIH-NINDS (NS096282, NS076352, and NS086604), NICHD (HD106197 and HD090256), the National Medical Research Council of Singapore (MOH-000212 and MOH-000207), Ministry of Education of Singapore (MOE2018-T2-2-103), Aligning Science Across Parkinson's (ASAP-000301) through the Michael J. Fox Foundation for Parkinson's Research (MJFF), the Bleser Family Foundation, and the Busta Foundation.

AUTHOR CONTRIBUTIONS

Y.Y. conceived and designed the study; performed the cell culture, differentiation, immunostaining, bioink preparation, printing, calcium and glutamate imaging, data analysis and interpretation; and wrote the manuscript. X.L., S.M., and Y.D. performed the electrophysiology. L.K. provided astrocytes and produced GCaMP6 virus. Y.G. and X.Z. produced iGluSnFR virus. Y.T., X.L., and A.B. performed data interpretation. S.-C.Z. conceived and designed the study, acquired the funding, supervised the study, performed data analysis and interpretation, and wrote the manuscript.

DECLARATION OF INTERESTS

The manuscript comes with a patent entitled "Methods for Printing Functional Human Neural Tissue" (Application#18/057,026). S.C.Z. is a co-founder of BrainXell, Inc.

Received: December 26, 2022
Revised: November 1, 2023
Accepted: December 11, 2023
Published: February 1, 2024

REFERENCES

1. Sousa, A.M.M., Meyer, K.A., Santpere, G., Gulden, F.O., and Sestan, N. (2017). Evolution of the human nervous system function, structure, and development. Cell *170*, 226–247.
2. Beaulieu-Laroche, L., Toloza, E.H.S., van der Goes, M.S., Lafourcade, M., Barnagian, D., Williams, Z.M., Eskandar, E.N., Frosch, M.P., Cash, S.S., and Harnett, M.T. (2018). Enhanced dendritic compartmentalization in human cortical neurons. Cell *175*, 643–651.e14.
3. Vasile, F., Dossi, E., and Rouach, N. (2017). Human astrocytes: structure and functions in the healthy brain. Brain Struct. Funct. *222*, 2017–2029.
4. Choi, S.H., Kim, Y.H., Hebisch, M., Sliwinski, C., Lee, S., D'Avanzo, C., Chen, H., Hooli, B., Asselin, C., Muffat, J., et al. (2014). A three-dimensional human neural cell culture model of Alzheimer's disease. Nature *515*, 274–278.
5. Madl, C.M., LeSavage, B.L., Dewi, R.E., Dinh, C.B., Stowers, R.S., Khariton, M., Lampe, K.J., Nguyen, D., Chaudhuri, O., Enejder, A., et al. (2017). Maintenance of neural progenitor cell stemness in 3D hydrogels requires matrix remodelling. Nat. Mater. *16*, 1233–1242.
6. Tang-Schomer, M.D., White, J.D., Tien, L.W., Schmitt, L.I., Valentin, T.M., Graziano, D.J., Hopkins, A.M., Omenetto, F.G., Haydon, P.G., and Kaplan, D.L. (2014). Bioengineered functional brain-like cortical tissue. Proc. Natl. Acad. Sci. USA *111*, 13811–13816.
7. Yan, Y., Li, Y., Song, L., Zeng, C., and Li, Y. (2017). Pluripotent stem cell expansion and neural differentiation in 3-D scaffolds of tunable Poisson's ratio. Acta Biomater. *49*, 192–203.
8. Bouyer, C., Chen, P., Güven, S., Demirtaş, T.T., Nieland, T.J., Padilla, F., and Demirci, U. (2016). A bio-acoustic levitational (BAL) assembly method for engineering of multilayered, 3D brain-like constructs, using human embryonic stem cell derived neuro-progenitors. Adv. Mater. *28*, 161–167.
9. Lancaster, M.A., Renner, M., Martin, C.A., Wenzel, D., Bicknell, L.S., Hurles, M.E., Homfray, T., Penninger, J.M., Jackson, A.P., and Knoblich, J.A. (2013). Cerebral organoids model human brain development and microcephaly. Nature *501*, 373–379.
10. Paşca, A.M., Sloan, S.A., Clarke, L.E., Tian, Y., Makinson, C.D., Huber, N., Kim, C.H., Park, J.Y., O'Rourke, N.A., Nguyen, K.D., et al. (2015). Functional cortical neurons and astrocytes from human pluripotent stem cells in 3D culture. Nat. Methods *12*, 671–678.
11. Vatine, G.D., Barrile, R., Workman, M.J., Sances, S., Barriga, B.K., Rahnama, M., Barthakur, S., Kasendra, M., Lucchesi, C., Kerns, J., et al. (2019). Human iPSC-derived blood-brain barrier chips enable disease modeling and personalized medicine applications. Cell Stem Cell *24*, 995–1005.e6.
12. Harberts, J., Fendler, C., Teuber, J., Siegmund, M., Silva, A., Rieck, N., Wolpert, M., Zierold, R., and Blick, R.H. (2020). Toward brain-on-a-chip: human induced pluripotent stem cell-derived guided neuronal networks in tailor-made 3D nanoprinted microscaffolds. ACS Nano *14*, 13091–13102.
13. Murphy, S.V., and Atala, A. (2014). 3D bioprinting of tissues and organs. Nat. Biotechnol. *32*, 773–785.
14. Qiu, B., Bessler, N., Figler, K., Buchholz, M.B., Rios, A.C., Malda, J., Levato, R., and Caiazzo, M. (2020). Bioprinting neural systems to model central nervous system diseases. Adv. Funct. Mater. *30*, 1910250.

15. Pagan-Diaz, G.J., Ramos-Cruz, K.P., Sam, R., Kandel, M.E., Aydin, O., Saif, M.T.A., Popescu, G., and Bashir, R. (2019). Engineering geometrical 3-dimensional untethered in vitro neural tissue mimic. Proc. Natl. Acad. Sci. USA *116*, 25932–25940.

16. Crowe, J.A., El-Tamer, A., Nagel, D., Koroleva, A.V., Madrid-Wolff, J., Olarte, O.E., Sokolovsky, S., Estevez-Priego, E., Ludl, A.A., Soriano, J., et al. (2020). Development of two-photon polymerised scaffolds for optical interrogation and neurite guidance of human iPSC-derived cortical neuronal networks. Lab Chip *20*, 1792–1806.

17. Koroleva, A., Deiwick, A., El-Tamer, A., Koch, L., Shi, Y., Estévez-Priego, E., Ludl, A.A., Soriano, J., Guseva, D., Ponimaskin, E., et al. (2021). In vitro development of human iPSC-derived functional neuronal networks on laser-fabricated 3D scaffolds. ACS Appl. Mater. Interfaces *13*, 7839–7853.

18. Lozano, R., Stevens, L., Thompson, B.C., Gilmore, K.J., Gorkin, R., 3rd, Stewart, E.M., in het Panhuis, M., Romero-Ortega, M., and Wallace, G.G. (2015). 3D printing of layered brain-like structures using peptide modified gellan gum substrates. Biomaterials *67*, 264–273.

19. Joung, D., Truong, V., Neitzke, C.C., Guo, S.Z., Walsh, P.J., Monat, J.R., Meng, F., Park, S.H., Dutton, J.R., Parr, A.M., et al. (2018). 3D Printed stem-cell derived neural progenitors generate spinal cord scaffolds. Adv. Funct. Mater. *28*, 1801850.

20. Noh, S., Kim, K., Kim, J.-I., Shin, J.H., and Kang, H.-W. (2020). Direct-write printing for producing biomimetic patterns with self-aligned neurites. Addit. Manuf. *32*, 101072.

21. Xu, T., Gregory, C.A., Molnar, P., Cui, X., Jalota, S., Bhaduri, S.B., and Boland, T. (2006). Viability and electrophysiology of neural cell structures generated by the inkjet printing method. Biomaterials *27*, 3580–3588.

22. Lee, W., Pinckney, J., Lee, V., Lee, J.H., Fischer, K., Polio, S., Park, J.K., and Yoo, S.S. (2009). Three-dimensional bioprinting of rat embryonic neural cells. NeuroReport *20*, 798–803.

23. Koser, D.E., Thompson, A.J., Foster, S.K., Dwivedy, A., Pillai, E.K., Sheridan, G.K., Svoboda, H., Viana, M., Costa, L.D., Guck, J., et al. (2016). Mechanosensing is critical for axon growth in the developing brain. Nat. Neurosci. *19*, 1592–1598.

24. Georges, P.C., Miller, W.J., Meaney, D.F., Sawyer, E.S., and Janmey, P.A. (2006). Matrices with compliance comparable to that of brain tissue select neuronal over glial growth in mixed cortical cultures. Biophys. J. *90*, 3012–3018.

25. Rademakers, T., Horvath, J.M., van Blitterswijk, C.A., and LaPointe, V.L.S. (2019). Oxygen and nutrient delivery in tissue engineering: approaches to graft vascularization. J. Tissue Eng. Regen. Med. *13*, 1815–1829.

26. Caliari, S.R., and Burdick, J.A. (2016). A practical guide to hydrogels for cell culture. Nat. Methods *13*, 405–414.

27. Hölzl, K., Lin, S., Tytgat, L., Van Vlierberghe, S., Gu, L., and Ovsianikov, A. (2016). Bioink properties before, during and after 3D bioprinting. Biofabrication *8*, 032002.

28. England, S., Rajaram, A., Schreyer, D.J., and Chen, X. (2017). Bioprinted fibrin-factor XIII-hyaluronate hydrogel scaffolds with encapsulated Schwann cells and their in vitro characterization for use in nerve regeneration. Bioprinting *5*, 1–9.

29. Hospodiuk, M., Dey, M., Sosnoski, D., and Ozbolat, I.T. (2017). The bioink: a comprehensive review on bioprintable materials. Biotechnol. Adv. *35*, 217–239.

30. Wonders, C.P., and Anderson, S.A. (2006). The origin and specification of cortical interneurons. Nat. Rev. Neurosci. *7*, 687–696.

31. Tremblay, R., Lee, S., and Rudy, B. (2016). GABAergic interneurons in the neocortex: from cellular properties to circuits. Neuron *91*, 260–292.

32. Shi, Y., Kirwan, P., Smith, J., Robinson, H.P., and Livesey, F.J. (2012). Human cerebral cortex development from pluripotent stem cells to functional excitatory synapses. Nat. Neurosci. *15*, 477–486.

33. Gunhanlar, N., Shpak, G., van der Kroeg, M., Gouty-Colomer, L.A., Munshi, S.T., Lendemeijer, B., Ghazvini, M., Dupont, C., Hoogendijk, W.J.G., Gribnau, J., et al. (2018). A simplified protocol for differentiation of electrophysiologically mature neuronal networks from human induced pluripotent stem cells. Mol. Psychiatry *23*, 1336–1344.

34. Nicholas, C.R., Chen, J., Tang, Y., Southwell, D.G., Chalmers, N., Vogt, D., Arnold, C.M., Chen, Y.J., Stanley, E.G., Elefanty, A.G., et al. (2013). Functional maturation of hPSC-derived forebrain interneurons requires an extended timeline and mimics human neural development. Cell Stem Cell *12*, 573–586.

35. Khakh, B.S., and Sofroniew, M.V. (2015). Diversity of astrocyte functions and phenotypes in neural circuits. Nat. Neurosci. *18*, 942–952.

36. Ben Haim, L., and Rowitch, D.H. (2017). Functional diversity of astrocytes in neural circuit regulation. Nat. Rev. Neurosci. *18*, 31–41.

37. Zhou, L., Wolfes, A.C., Li, Y., Chan, D.C.W., Ko, H., Szele, F.G., and Bayley, H. (2020). Lipid-bilayer-supported 3D printing of human cerebral cortex cells reveals developmental interactions. Adv. Mater. *32*, e2002183.

38. Salaris, F., Colosi, C., Brighi, C., Soloperto, A., Turris, V., Benedetti, M.C., Ghirga, S., Rosito, M., Di Angelantonio, S., and Rosa, A. (2019). 3D bioprinted human cortical neural constructs derived from induced pluripotent stem cells. J. Clin. Med. *8*, 1595.

39. Dong, Y., Xiong, M., Chen, Y., Tao, Y., Li, X., Bhattacharyya, A., and Zhang, S.C. (2020). Plasticity of synaptic transmission in human stem cell-derived neural networks. iScience *23*, 100829.

40. Dana, H., Mohar, B., Sun, Y., Narayan, S., Gordus, A., Hasseman, J.P., Tsegaye, G., Holt, G.T., Hu, A., Walpita, D., et al. (2016). Sensitive red protein calcium indicators for imaging neural activity. eLife *5*, e12727.

41. Messing, A., Brenner, M., Feany, M.B., Nedergaard, M., and Goldman, J.E. (2012). Alexander disease. J. Neurosci. *32*, 5017–5023.

42. Jones, J.R., Kong, L., Hanna, M.G.t., Hoffman, B., Krencik, R., Bradley, R., Hagemann, T., Choi, J., Doers, M., Dubovis, M., et al. (2018). Mutations in GFAP disrupt the distribution and function of organelles in human astrocytes. Cell Rep. *25*, 947–958.e4.

43. Mignot, C., Boespflug-Tanguy, O., Gelot, A., Dautigny, A., Pham-Dinh, D., and Rodriguez, D. (2004). Alexander disease: putative mechanisms of an astrocytic encephalopathy. Cell. Mol. Life Sci. *61*, 369–385.

44. Edelbrock, A.N., Clemons, T.D., Chin, S.M., Roan, J.J.W., Bruckner, E.P., Álvarez, Z., Edelbrock, J.F., Wek, K.S., and Stupp, S.I. (2021). Superstructured biomaterials formed by exchange dynamics and host-guest interactions in supramolecular polymers. Adv. Sci. (Weinh) *8*, 2004042.

45. Kajtez, J., Wesseler, M.F., Birtele, M., Khorasgani, F.R., Rylander Ottosson, D., Heiskanen, A., Kamperman, T., Leijten, J., Martínez-Serrano, A., Larsen, N.B., et al. (2022). Embedded 3D printing in self-healing annealable composites for precise patterning of functionally mature human neural constructs. Adv. Sci. (Weinh) *9*, e2201392.

46. Skylar-Scott, M.A., Huang, J.Y., Lu, A., Ng, A.H.M., Duenki, T., Liu, S., Nam, L.L., Damaraju, S., Church, G.M., and Lewis, J.A. (2022). Orthogonally induced differentiation of stem cells for the programmatic patterning of vascularized organoids and bioprinted tissues. Nat. Biomed. Eng. *6*, 449–462.

47. Miura, Y., Li, M.Y., Birey, F., Ikeda, K., Revah, O., Thete, M.V., Park, J.Y., Puno, A., Lee, S.H., Porteus, M.H., et al. (2020). Generation of human striatal organoids and cortico-striatal assembloids from human pluripotent stem cells. Nat. Biotechnol. *38*, 1421–1430.

48. Xiang, Y., Tanaka, Y., Patterson, B., Kang, Y.J., Govindaiah, G., Roselaar, N., Cakir, B., Kim, K.Y., Lombroso, A.P., Hwang, S.M., et al. (2017). Fusion of regionally specified hPSC-derived organoids models human brain development and interneuron migration. Cell Stem Cell *21*, 383–398.e7.

49. Andersen, J., Revah, O., Miura, Y., Thom, N., Amin, N.D., Kelley, K.W., Singh, M., Chen, X., Thete, M.V., Walczak, E.M., et al. (2020). Generation of functional human 3D cortico-motor assembloids. Cell *183*, 1913–1929.e26.

50. Tao, Y., and Zhang, S.C. (2016). Neural subtype specification from human pluripotent stem cells. Cell Stem Cell *19*, 573–586.

51. Li, X., Tao, Y., Bradley, R., Du, Z., Tao, Y., Kong, L., Dong, Y., Jones, J., Yan, Y., Harder, C.R.K., et al. (2018). Fast generation of functional subtype astrocytes from human pluripotent stem cells. Stem Cell Rep. *11*, 998–1008.

52. Yan, Y., Martin, L.M., Bosco, D.B., Bundy, J.L., Nowakowski, R.S., Sang, Q.X., and Li, Y. (2015). Differential effects of acellular embryonic matrices on pluripotent stem cell expansion and neural differentiation. Biomaterials *73*, 231–242.

53. Yan, Y., Song, L., Madinya, J., Ma, T., and Li, Y. (2018). Derivation of cortical spheroids from human induced pluripotent stem cells in a suspension bioreactor. Tissue Eng. Part A *24*, 418–431.

54. Yan, Y., Bejoy, J., Xia, J., Guan, J., Zhou, Y., and Li, Y. (2016). Neural patterning of human induced pluripotent stem cells in 3-D cultures for studying biomolecule-directed differential cellular responses. Acta Biomater. *42*, 114–126.

55. Liu, Y., Liu, H., Sauvey, C., Yao, L., Zarnowska, E.D., and Zhang, S.C. (2013). Directed differentiation of forebrain GABA interneurons from human pluripotent stem cells. Nat. Protoc. *8*, 1670–1679.

56. Liu, Y., Weick, J.P., Liu, H., Krencik, R., Zhang, X., Ma, L., Zhou, G.M., Ayala, M., and Zhang, S.C. (2013). Medial ganglionic eminence-like cells derived from human embryonic stem cells correct learning and memory deficits. Nat. Biotechnol. *31*, 440–447.

57. Ma, L., Hu, B., Liu, Y., Vermilyea, S.C., Liu, H., Gao, L., Sun, Y., Zhang, X., and Zhang, S.C. (2012). Human embryonic stem cell-derived GABA neurons correct locomotion deficits in quinolinic acid-lesioned mice. Cell Stem Cell *10*, 455–464.

58. Krencik, R., Weick, J.P., Liu, Y., Zhang, Z.J., and Zhang, S.C. (2011). Specification of transplantable astroglial subtypes from human pluripotent stem cells. Nat. Biotechnol. *29*, 528–534.

59. Kubota, K., Kogure, H., Masuda, Y., Toyama, Y., Kita, R., Takahashi, A., and Kaibara, M. (2004). Gelation dynamics and gel structure of fibrinogen. Colloids Surf. B Biointerfaces *38*, 103–109.

60. Sproul, E.P., Hannan, R.T., and Brown, A.C. (2018). Controlling fibrin network morphology, polymerization, and degradation dynamics in fibrin gels for promoting tissue repair. Methods Mol. Biol. *1758*, 85–99.

61. Kolesky, D.B., Homan, K.A., Skylar-Scott, M.A., and Lewis, J.A. (2016). Three-dimensional bioprinting of thick vascularized tissues. Proc. Natl. Acad. Sci. USA *113*, 3179–3184.

62. Goldman, J.S., Ashour, M.A., Magdesian, M.H., Tritsch, N.X., Harris, S.N., Christofi, N., Chemali, R., Stern, Y.E., Thompson-Steckel, G., Gris, P., et al. (2013). Netrin-1 promotes excitatory synaptogenesis between cortical neurons by initiating synapse assembly. J. Neurosci. *33*, 17278–17289.

63. Cheng, C., Lau, S.K., and Doering, L.C. (2016). Astrocyte-secreted thrombospondin-1 modulates synapse and spine defects in the fragile X mouse model. Mol. Brain *9*, 74.

64. Gao, Y., Shen, M., Gonzalez, J.C., Dong, Q., Kannan, S., Hoang, J.T., Eisinger, B.E., Pandey, J., Javadi, S., Chang, Q., et al. (2020). RGS6 mediates effects of voluntary running on adult hippocampal neurogenesis. Cell Rep. *32*, 107997.

65. Marvin, J.S., Borghuis, B.G., Tian, L., Cichon, J., Harnett, M.T., Akerboom, J., Gordus, A., Renninger, S.L., Chen, T.W., Bargmann, C.I., et al. (2013). An optimized fluorescent probe for visualizing glutamate neurotransmission. Nat. Methods *10*, 162–170.

66. Sloan, S.A., Darmanis, S., Huber, N., Khan, T.A., Birey, F., Caneda, C., Reimer, R., Quake, S.R., Barres, B.A., and Paşca, S.P. (2017). Human astrocyte maturation captured in 3D cerebral cortical spheroids derived from pluripotent stem cells. Neuron *95*, 779–790.e6.

STAR★METHODS

KEY RESOURCES TABLE

REAGENT or RESOURCE	SOURCE	IDENTIFIER
Antibodies		
Rabbit Calbindin	Abcam	ab25085, RRID: AB_448597
Rabbit Calretinin	Epitomics Inc.	2624-1, RRID:AB_2228336
Rat CTIP2	Abcam	ab18465, RRID: AB_2064130
Rabbit DARPP32	Abcam	Ab40801, RRID: AB_731843
Rabbit DARPP32	Millipore Sigma	AB10518, RRID: AB_10807019
Rabbit Drebrin	Millipore	AB10140, RRID: AB_1977159
Rabbit FOXG1	Abcam	ab18259, RRID: AB_732415
Rabbit GABA	Sigma	A2052, RRID: AB_2314459
Mouse Gephyrin	Synaptic Systems	147011, RRID: AB_2810215
Mouse GFAP	Millipore	IF03L, RRID: AB_2294571
Rabbit GFAP	Dako	Z033429, RRID:AB_10013382
Mouse GLT1	BD Transduction Laboratories	611654, RRID: AB_399172
Mouse GFP	Millipore	MAB3580, RRID: AB_94936
Rabbit GFP	Millipore Sigma	AB3080, RRID: AB_91337
Chicken GFP	Novus Biologicals	NB100-1614, RRID: AB_10001164
Rabbit MAP2	Millipore	AB5622, RRID: AB_91939
Mouse MAP2	Sigma	M1406-2ML, RRID: AB_477171
Chicken MAP2	Abcam	ab5392, RRID: AB_2138153
Rat mCherry	ThermoFisher Scientific	M11217, RRID: AB_2536611
Mouse NeuN	Millipore	MAB377, RRID: AB_2298772
Mouse NKX2.1	Millipore	MAB5460, RRID: AB_571072
Goat OTX2	R&D System	AF1979, RRID: AB_2157172
Mouse Parvalbumin	Millipore	MAB1572, RRID: AB_2174013
Mouse PAX6	DSHB	PAX6, RRID: AB_528427
Mouse PSD95	Synaptic Systems	124011, RRID: AB_2619799
Mouse S100β	Abcam	ab11178, RRID: AB_297817
Mouse SATB2	Abcam	ab51502, RRID: AB_882455
Mouse SMI312	BioLegend	837904, RRID: AB_2566782
Rat Somatostatin	Millipore	MAB354, RRID: AB_2255365
Rabbit SOX2	Millipore	AB5603, RRID: AB_2286686
Rabbit SYN1	Synaptic Systems	106-003, RRID: AB_2619773
Rabbit TBR1	Abcam	ab31940, RRID: AB_2200219
Rabbit TUJ1	Covance	PBR-435P, RRID: AB_291637
Mouse TUJ1	Abcam	Ab78078, RRID: AB_2256751
Rabbit vGAT	Synaptic Systems	131002, RRID: AB_887871
Rabbit vGlut1	Synaptic Systems	135303, RRID: AB_887875
Chemicals and proteins		
Accutase	Innovative Cell Technologies, Inc.	AT-104
Aprotinin	Sigma	A1153
B27 supplement w/o Vitamin A	Thermo Fisher Scientific	12587-010
Bicuculline methiodide	Tocris	2503
Bovine serum albumin (BSA)	VMR	10842-772
$CaCl_2$	Sigma	C7902
c-AMP	Sigma-Aldrich	D0627

(*Continued on next page*)

Continued

REAGENT or RESOURCE	SOURCE	IDENTIFIER
Cyclopamine	Stemgent	04-0022
D-(+)-Glucose	Sigma	G8270-1KG
Dispase	Thermo Fisher Scientific	17105-041
DMEM/F12 basal medium	Thermo Fisher Scientific	11330-032
DMH1	Tocris	4126
DPBS	Thermo Fisher Scientific	141901144
EGF	R&D Systems	236-EG-01M
EGTA	Sigma	E3889-500G
FGF-2	R&D Systems	233-FB-500/CF
Fibrinogen	Sigma	F3879
Gelatin	Sigma	G9391-500G
GlutaMAX	Gibco	35050-079
GTP-Na	Sigma	10106399001
HEPES (1 M)	Thermo Fisher Scientific	15630080
Hoechst 33342	Thermo Fisher Scientific	R37165
Hyaluronic acid	Sigma	53747
KnockOut Serum Replacement	Thermo Fisher Scientific	10828028
L-Ascorbic acid	Tocris	4055
LDN193189	Sigma	SML0559-5MG
L-glutamine	Thermo Fisher Scientific	25030-081
Lyophilized moo glue powder	Modernist Pantry	N/A
Magnesium chloride	Sigma	M8266-100G
Matrigel	BD Biosciences	354277
Methyl cellulose,viscosity 15 cPs	Alfa Aesar	45490-22
N2 Supplement	Thermo Fisher Scientific	17502-048
Neurobasal medium	Gibco	21103-049
Non-essential Amino Acids	Thermo Fisher Scientific	11140050
Paraformaldehyde	Sigma	P6148-1KG
Phosphocreatine	Sigma	P7936
Potassium chloride	Sigma	P3911-500G
Purmorphamine	Tocris	4551
Recombinant human BDNF	Peprotech	450-02
Recombinant human GDNF	Peprotech	450-10
ROCK inhibitor Y27632	Stemcell Tech.	72304
SB431542	Stemgent	04-0010-10
Shh C25II	R&D Systems	464-SH-01M
Sodium alginate	Sigma	W201502
Sodium chloride	Sigma	S9888-500G
Sucrose	Sigma	S9378-1KG
TeSR-E8 medium	Stemcell Tech.	05991
Thrombin	Sigma	T7009
Triton-X100	Sigma	X100-500ML
UltraPure 0.5 M EDTA	Life Technologies	15575-038
VPA	Sigma	P4543
β-mercaptoethanol	Sigma	M7522-100ML
Critical commercial assays		
Lenti-X Concentrator	TakaRa Bio	631232
Lenti-X GoStix Plus	TakaRa Bio	631280
Live/Dead staining kit	Thermo Fisher Scientific	R37601

(*Continued on next page*)

Continued

REAGENT or RESOURCE	SOURCE	IDENTIFIER
Recombinant DNA		
pAAV.Syn.NES-jRGECO1b.WPRE.SV40	Addgene	100857
pDM2.g	Addgene	12259
pENN.AAV.GFAP.iGluSnFr.WPRE.SV40	Addgene	98930
psPax2	Addgene	12260
Experimental models: Cell lines		
Human: H9 ES cells	WiCell Research Institute	WA09
Human: Syn-GFP-H9 ES cells	WiCell Research Institute	NIHhESC-10-0062
Human: WIZ04e-CAG-mCherry-H9 ES cells	WiCell Research Institute	WIZ04e
Human: CAG-ChR2-YFP-H9 ES cells	WiCell Research Institute	WAe009-A-29
Human: AxD R88C iPS cells	Waisman center iPSC core	WC-01-01-AL-AM
Human: HEK-293T	CCHMC Pluripotent Stem cell core / ATCC	CRL-3216
Software		
CorelDraw	Alludo	N/A
Excel	Microsoft	2013
Igor	WaveMetrics	v4.0
ImageJ&FIJI	NIH	N/A
Imaris	Oxford Instruments	v10.1
MiniAnalysis	WaveMetrics	v6.0
Notepad++7	Microsoft	v7
pClamp	Molecular Devices	v11.0.3
Prism	GraphPad	v5&v8
Repetier Host	Hot-World GmbH & Co. KG	v2.0.5
Slic3r	N/A	v3
Other		
6-Well tissue culture plates	Thermo Fisher Scientific	140675
24-Well tissue culture plates	Thermo Fisher Scientific	142475
27G Micronozzle	Cellink	NZ3270005001
30G Microneedle	Cellink	NZ5300505001
3 mL Cartridge	Cellink	CSC010311101

RESOURCE AVAILABILITY

Lead contact

Further information and requests for resources and reagents should be directed to and will be fulfilled by the lead contact, Dr. Su-Chun Zhang (suchun.zhang@wisc.edu).

Materials availability

All plasmids and human pluripotent stem cells lines generated in the study are available at Addgene (https://www.addgene.org/) and WiCell Research Institute (https://www.wicell.org/) or upon request with appropriate MTA. They are listed in the key resources table. This study did not generate new unique reagents. Reagents generated in this study will be made available on request, but we may require a payment and/or a completed MTA if there is potential for commercial application.

Data and code availability

The G.code for the design of print construct is available in the Data S1 file. Any additional information required to reanalyze the data reported in this paper is available from the lead contact upon request.

EXPERIMENTAL MODEL AND STUDY PARTICIPANT DETAILS

Human cell source

Human ESCs (H9, GFP-H9, mCherry-H9, and ChR2-EYFP) and iPSCs (AxD R88C and isogenic control) were maintained on the mouse embryonic fibroblast (MEF) feeder in a stem cell growth medium or on Matrigel-coated plates in the TeSR-E8 medium (StemCell Technologies, Inc., Vancouver, Canada) as described previously.[51,52] For MEF feeder-based cultures, cells were passaged weekly by using dispase (1 mg/mL) and plating on a monolayer of irradiated MEF (WiCell). The hPSC culture medium consisted of DMEM/F12 basal medium (Gibco), 20% KnockOut serum replacement (Gibco), 0.1 mM β-mercaptoethanol (Sigma), 1 mM L-glutamine (Gibco), nonessential amino acids (Gibco), and 4 ng/mL fibroblast growth factor (FGF)-2 (R&D Systems). For TeSR-E8 medium-based cultures, cells were passaged every 6-7 days by accutase and plated on Matrigel-coated 6-well plates for monolayer cultures in the presence of ROCK inhibitor Y27632 (10 μM) to promote cell survival.

METHOD DETAILS

Generation of cortical neural progenitors, GABAergic interneurons, striatal neurons, and astrocyte progenitors from hPSCs

The generation of cortical neural progenitors was performed as previously described.[53,54] Briefly, hPSCs were seeded into Ultra-Low Attachment (ULA) 24-well plates (Corning, Inc., Corning, NY) at 3.0 – 3.5 $\times 10^5$ cells per well in 1mL of TeSRE8 medium and grown for 2 days. ROCK inhibitor Y27632 (10 μM) was added during the seeding and removed after 24 h. Then, the culture was switched to the neural differentiation medium composed of Dulbecco's modified Eagle's medium/nutrient mixture F-12 (DMEM/F12) plus 2% B27 w/o vitamin A serum-free supplement. At day 1 in the neural differentiation medium, the cells were treated with dual SMAD signaling inhibitors: 10 μM SB431542 and 100nM LDN193189 (Sigma). After 7 days, the cells were incubated with cyclopamine (1 μM, Stemgent), FGF-2 (10 ng/mL, R&D System) and epidermal growth factor (EGF, 10 ng/mL, R&D System) for another 8 days. The cell cultures were maintained in FGF-2 until day 21 in suspension and were dissociated by accutase for printing.

The differentiation of GABAergic interneurons was based on our developed protocol.[55,56] After 7 days of the above neural differentiation, the sonic hedgehog (SHH) activator purmorphamine (1 μM, Tocris) was added. At day 21, the GABAergic interneuron progenitors were also dissociated to single cells for printing.

The striatal DARPP32$^+$ neurons or medium spiny neurons were generated using our previous protocol.[57] Briefly, 40 ng/mL SHH C25II (R&D Systems) was added to the neural differentiation medium from day 7 to day 25 after one week of dual SMAD signaling inhibitors treatment. At day 25, the striatal progenitors were then treated with VPA (10μM, Sigma) for 5 days. And single striatal neurons were prepared for printing.

The generation of astrocyte progenitors was performed from our previous protocol.[51,58] Briefly, hPSCs were treated with dual SMAD inhibitors to generate neuroepithelia for 14 days on a monolayer culture. On day 14, neuroepithelia were lifted after brief treatment with 500 μM EDTA (Life Technologies), and resuspended DMEM/F12 plus 1% N2 supplement and FGF-2 (10 ng/mL, R&D System). Half medium change was performed every two to three days. On day 30, EGF (10 ng/mL, R&D System) was added to encourage the expansion of glial progenitors till day 180. And single astrocyte progenitors were prepared for printing.

Preparation of fibrin gel

Stock solution of 50 mg/mL fibrinogen, 100 U thrombin, 250 mM $CaCl_2$ (100X) and 10 mg/mL aprotinin (20X) were prepared in the following manner: Fibrinogen (F3879, Sigma) was dissolved in Dulbecco's phosphate buffered saline (DPBS) without calcium and magnesium for 4 h at 37°C. The solution was sterile-filtered and stored at -80°C for use. $CaCl_2$ (Sigma) was dissolved in deionized (DI) water and filtered for use. Thrombin (T7009, Signa) was dissolved in DPBS and sterile-filtered. The solution was stored at -20°C until use. Aprotinin (A1153, Sigma) was dissolved in DPBS and stored at -20°C until use.

Culturing neural cells in fibrin gel

Dissociated hPSC-NPCs at a density of 1 × 10^6 were mixed with fibrinogen at the following concentrations (1, 2.5, 5, 10 and 20 mg/mL). 0.5 mg/mL aprotinin was added for preventing gel degradation. 1 μL of the fibrinogen-laden cells were dropped on the poly-ornithine coated plates at RT (room temperature). And 1 μL of different concentrations of thrombin (0.5, 1, 25,5 and 10 U) solution with 2.5 mM $CaCl_2$ were then added and mixed with the cell-fibrinogen solution. Fresh medium was added after gelation. Cells were encapsulated in the fibrin gel constructs and cultured at 37°C incubator for characterizations.

Gelation testing of fibrin gel

The gelation testing of the fibrin gel was modified from previously reports.[59,60] Different concentrations of fibrinogen solutions and thrombin solutions were prepared. 1 μL fibrinogen solution was dropped onto cover slide and was mixed well with the same volume of thrombin. To test the gelation, a pipette tip of 2 μL was used to touch the gel to check whether the gel was solid or not (no liquid could be taken by the pipette tip). And the time from the addition of thrombin and formation of the gel was recorded. We defined it the gelation time.

Bioink preparation

The four groups of hydrogel mixtures (Table S1) were used in this study for cell-laden bioinks: gelatin/alginate/fibrinogen (GLN + ALG + FN), alginate/nanofibrillate cellulose/fibrinogen (ALG + NFN + FN), Matrigel/fibrinogen (MG + FN), and hyaluronic acid/fibrinogen (HA + FN). The crosslinking solution was $CaCl_2$ + thrombin + transglutaminase (TG). All the bioinks were based on the formation of fibrin gel. The final concentrations of fibrinogen and thrombin in the fibrin gel constructs were maintained at 2. 5 mg/mL and 0.5 U, respectively. All the cells used for printing were disaggregated and were filtered using 30 μm CellTrics disposable filter (04-004-2326, Sysmex)to avoid nozzle clogging. Cells were counted through hemocytometer and were prepared at a density of 1×10^7/ mL.

Crosslinking buffer $CaCl_2$ + thrombin + transglutaminase (TG) was prepared as following: The TG solution was created as a previously published protocol.[19,61] Lyophilized Moo Glue powder (Modernist Pantry; ME, USA) was prepared in DPBS and stirring at 37°C until completely dissolved to make 60 mg/mL solution. The final working crosslinking solution contained 2.5 mM $CaCl_2$, 1U thrombin and 0.2 % (w/v) of TG. The crosslinking was performed at 3-5 min at room temperature (RT). To avoid dehydration of gel, the crosslinking agent was added immediately after printing. The volume of the crosslinking solution was equal to the volume of bioinks.

The GLN + ALG + FN was hydrogel mixture of gelatin (GLN), alginate (ALG) and fibrinogen (FN) at a ratio of 2: 1 :1 by volume. Gelatin (G6411, Sigma) was dissolved in DPBS for 12 h at 90°C to make 120 mg/mL stock solution. The solution was stored at 4°C until use. 3% (w/v) of low viscosity alginate (A18565, Alfa Aesar) was prepared in DPBS without calcium and magnesium. The fibrinogen stock (50 mg/mL) was diluted by fresh neural differentiation medium to make 20 mg/mL for use. For printing test, hPSC-NPCs at day 21 were dissociated by accutase and filtered to make single cells. The cells were centrifuged and resuspended with 20 mg/mL fibrinogen solution at a density of 1×10^7/mL. The cell-fibrinogen solution was then mixed with 120 mg/mL gelation and 3% (w/v) alginate solution at a volume ratio of 2: 1: 1. The bioink was prepared freshly before printing. The printing was performed at 10°C. After printing, the hydrogel was crosslinked with a thrombin + transglutaminase (TG) + $CaCl_2$ for 10-15 min at 10°C. And fresh medium was added after crosslinking for post-printing culture at 37°C for characterizations.

The ALG + NFN + FN hydrogel mixture, created from 3% (w/v) alginate solution (ALG), 10 % (w/v) nanofibrillate cellulose (NFN) and 15 mg/mL fibrinogen with a volume ratio of 1: 1: 1. 10 % (w/v) NFN (methyl cellulose, viscosity 15 cPs, 45490, Alfa Aesar), was dissolved in DPBS. The printing was performed at RT. After printing, the hydrogel was crosslinked with a thrombin + transglutaminase (TG) + $CaCl_2$ for 3-5 min at RT. And fresh medium was added after crosslinking at 37°C for characterizations.

The MG + FN bioink was prepared from 10 mg/mL fibrinogen solution and Matrigel (BD Biosciences) with a volume ratio of 1: 1. Briefly, cells were centrifuged and resuspended with 10 mg/mL fibrinogen solution at a density of 1×10^7/mL. And Matrigel was added to make the final cell-laden bioink. The printing and crosslinking were performed at RT.

The HA + FN bioink was made of hyaluronic acid (HA) (53747, Sigma) and 10 mg/mL fibrinogen with a volume ratio of 1: 2. 3% (w/v) HA was prepared in DPBS at 37°C and stirred until completely dissolved. The printing was performed at RT. After printing, the hydrogel was crosslinked with a thrombin + transglutaminase (TG) + $CaCl_2$ for 3-5 min at RT. And fresh medium was added after crosslinking at 37°C for characterizations.

Cell viability assay

Cell viability was indicated by the percent of live cells to total cells from Live/Dead assay. Live/Dead staining kit (Molecular Probes) was used to assess cell viability. Immediately after harvesting, the cells were incubated in DMEM/F12 containing 1 μM calcein AM and 2 μM ethidium homodimer I for 30 min. Cells were washed and representative images were taken. The number of live (green) and dead (red) cells were counted in each field using Cell Counter in Image-J. The live/dead cell numbers from the five images of one sample were averaged to give each data point and ten samples from three different batches were used to determine the viability.

Printing procedure

The printers were from CELLINK, INKREDIBLE+ and BioX (https://www.cellink.com/bioprinting/bio-x/). The printers had two or three printheads, which could deposit multiple types of cells at the same time. The dispensing apparatuses were connected to the printer to extrude different bioinks through the micronozzle with different inner diameters. Before printing, the UV light was turned on for 5 min to make sterile environment for printing. The printing seed, printing pressure and sizes of nozzle were optimized by measurement of the width of printed tissue layer. For printing structure test, we used CELLINK Start bioink without cells. The micronozzle was 27G (NZ3270005001, Cellink) with a 200 μm inner diameter. The printing speed for the Start bioink was at 3 mm/s (line-dispensing printing mode) and printing pressure was 50 kPa. For the printing with cell-laden bioinks, we performed a printing speed of 5 mm/s (line-dispensing printing mode) and printing pressure of 100 kPa using the blunt needle of 30G (NZ5300505001, Cellink, inner diameter 150 μm) or blunt needle of 27G (NZ6270505001, Cellink, inner diameter 200 μm). All the print paths were controlled using G-code commands, which were generated by the software Slic3R from 3 models.

Printing neural tissues

For printing the layered tissue using colored cells (GFP- and mCherry-labeled) or unlabeled cells, neural cells (glutamate neuron progenitors, GABA neuron progenitors, striatal neuron progenitors and astrocyte progenitors) were dissociated and filtered to make single cells. They were prepared separately and laden with the HA + FN bioink at a density of 1×10^7/mL. The gel-laden cells were delivered to two different nozzles and deposited onto poly-ornithine coated coverslips. The crosslinking solution was added immediately after printing. The gelation was performed at RT. Printed tissues were incubated at 37°C in the fresh neural differentiation medium for

the following experiments. At day 0 post-printing, printed tissues were cultured in neural basal medium plus 2% B-27 serum-free supplement, 10 ng/mL BDNF (brain-derived neurotrophic factor), 10 ng/mL GDNF (glial cell line derived neurotrophic factor), 200 μM AA (ascorbic acid), and 1 μM cAMP. For the printed tissue with astrocytes, 10 ng/mL CNTF (ciliary neurotrophic factor) was added as well. ROCK inhibitor Y27632 (10 μM) was added for the first 24 h. The medium was changed every 3 days.

Immunofluorescence and quantification

Cells on coverslips or wells were rinsed with PBS and fixed in 4% paraformaldehyde for 20 min. After rinsing with PBS twice, cells were treated with 0.3% Triton for 10 min followed by 10% donkey serum for 1 hour before incubating with primary antibodies overnight at 4°C. Cells were then incubated for 1h at room temperature with secondary antibodies. The nuclei were stained with Hoechst 33342 (Hoe) (Sigma-Aldrich). Please see key resources table for list of antibodies. Images were taken with a Nikon A1R-Si laser-scanning confocal microscope (Nikon, Tokyo, Japan). The primary antibodies used were listed in Table S2. Cell quantification was previously described.[58] Briefly, multiple fields were chosen randomly under the fluorescent filter for nuclear staining throughout the coverslips in areas which contained a similar density of Hoe^+ cells and the total cells were counted. The fluorescent filters were shifted during imaging to count the cells labeled by different antibodies in the same field in the same manner. The quantitative data were repeated for three biological replicates.

Synaptic puncta quantification

The synaptic puncta analysis was performed as previously described.[62,63] Briefly, synapses were identified by the co-localization of the pre- and post-synaptic puncta and 100 μm of neurite proximal to the cell soma was selected for analysis using ImageJ. Images were thresholded using a constant value for each channel to remove low frequency background, and an image generated using the co-localization highlighter to identify regions of overlap between the labeling. Puncta were analyzed in each individual channel and in the co-localization image. About 30 neurons were collected for each condition, and each experiment was repeated for three biological replicates.

Lenti-GCaMP6 virus preparation

GCaMP6 lentiviral particles were produced in HEK293FT cells with a 2nd generation lentiviral system. Transfection and lentiviral collection were conducted by Lipofectamine 3000 reagent for lentiviral production. In brief, 7×10^6 HEK293FT cells were seeded on a 10cm plate the day prior to transfection. Next day, the cells were transfected with 4.3 μg of GCaMP6 transfer vector along with 10 μg of the packaging plasmid psPax2 and 3 μg the envelope plasmid pDM2.g (psPax2 [Addgene plasmid #12260] and pDM2.g [Addgene plasmid #12259] were gifts from Didier Tronto). Supernatants containing lentiviral particles were collected 24 hours and 52 hours post-transfection. The success of lentiviral production was confirmed using Lenti-X GoStix (TakaRa Bio) following manufacturer's instructions. The supernatant was then combined and concentrated with Lenti-X Concentrator (TakaRa Bio). Concentrated lentiviral particles were resuspended in DPBS with 0.1%BSA, aliquoted and stored at -80°C.

Lenti-jRGECO1b and lenti-iGluSnFR virus preparation

Lenti-EF1-jRGECO1b and lenti-EF1-iGluSnFR were cloned using lenti-CMV-GFP vector as a backbone[64] and the CMV-GFP cassette was replaced with EF1-jRGECO1b and EF1-iGluSnFR, respectively. The jRGECO1b was cloned from pAAV.Syn.NES-jRGECO1b.WPRE.SV40 vector (addgene plasmid #100857).[65] And the iGluSnFR was cloned from pENN.AAV.GFAP.iGluSnFr.WPRE.SV40 vector (addgene plasmid #98930). The sequence of the inserted cassette was confirmed by sequencing. Lentivirus production was performed as described previously[64] with modifications. Briefly, the viral transfer vector DNA and packaging plasmid DNA were co-transfected into HEK293T cells using PEI. The medium containing lentivirus was collected at 36, 60 and 84 h post-transfection, pooled, filtered through a 0.2-μm filter, and concentrated using an ultracentrifuge at 19,400 rpm for 2 h at 4°C using a SW32Ti rotor (Beckman). The virus was washed once and then resuspended in 50 μl PBS. We routinely obtained 5×10^8 infectious viral particles /ml for lentivirus.

Calcium and Glutamate imaging

Human PSC-derived astrocyte progenitors at day 180 were infected with Lenti-GCaMP6 or Lenti-iGluSnFR. After 3 days, the virus infected astrocyte progenitors were washed and then printed with hPSC-derived cortical and MGE progenitors at ratio of 4: 5: 1. Calcium or glutamate imaging was performed as previously described.[66] Briefly, the printed tissues were washed with low potassium Tyrode's solution (Low-KCl) (2 mM KCl, 129 mM NaCl, 2 mM $CaCl_2$, 1 mM $MgCl_2$, 30 mM glucose, 25 mM HEPES, 0.1% and Bovine Serum Albumin, pH 7.4) three times and incubated with the solution for 30 min at 37°C. When imaging, the sample was placed on the stage of confocal fluorescence microscope (A1, Nikon). A high potassium Tyrode's solution (High-KCl) (67 mM KCl, 67 mM NaCl, 2 mM $CaCl_2$, 1 mM $MgCl_2$, 30 mM glucose, 25 mM HEPES, 0.1% and Bovine Serum Albumin, pH 7.4) was then applied. As a control, the virus infected astrocyte progenitors were also cultured alone for the same period and High-KCl solution was applied. ImageJ was used for the following analysis. The fluorescence change was defined as $\Delta F/F(t) = (F_0\text{-}F(t))/F_0$, where F_0 is the average fluorescence intensity of the imaging area for samples in the Low-KCl solution, F(t) was the fluorescence intensity at a given time. The ΔF/F of the printed tissue was normalized by comparison of the ΔF/F of the control.

Optogenetic stimulation

Human PSC-derived striatal neuron progenitors at day 21 were infected with Lenti- jRGECO1b. After 3 days, the virus infected striatal progenitors were then printed with hPSC-ChR2-EYFP derived cortical progenitors. Optogenetic stimulation was performed as previously described.[39] Briefly, the printed cortical and striatal tissues were placed in a 35-mm glass-botton dish in neural medium and imaged using confocal fluorescence microscope (A1, Nikon). For optogenetic stimulation, ChR2-cells were activated with 470 nm light using a custom-made LED device (1 Watts, 470 nm; Cree lighting Inc.) coupled to a fiber optic cable. jRGECO1b was imaged at a rate of 4.6 frames per second. Stimulation experiments included 1450 frames, and 470 nm LED light was applied every 200 - 300 frames. ImageJ was used for the Ca^{2+} wave analysis.

Electrophysiology

Whole-cell patch-clamp recordings were made from human PSC-derived cortical glutamatergic and GABAergic neurons. The bath solution consisted of 135 mM NaCl, 3 mM KCl, 2 mM CaCl2, 1 mM MgCl2, 10 mM HEPES, 11 mM glucose, 10 mM sucrose, pH7.4. Recording pipettes were filled with an intracellular solution containing 120 mM potassium D-gluconate, 1 mM ethylene glycol-bis (β-aminoethyl ether) N,N,N',N'-tetraacetic acid (EGTA), 10 mM 4-(2-hydroxyethyl)piperazine-1-ethanesulfonic acid (HEPES), 4 mM ATP-Mg, 0.3 mM GTP-Na, 10 mM phosphocreatine, 0.1 mM CaCl2, 1 mM MgCl2, pH 7.2, 280–290 mOsm/L. Printed tissues on the coverslips were transferred into a perfusion chamber. Individual cells were visualized with the help of an infrared differential interference contrast (IR-DIC) Olympus BX51WI microscope at 40× water-immersion objective, and different cell types were further identified by their fluorescence detected with a CCD camera and displayed on a monitor. Recording pipettes were made by pulling the glass (BF150-86-10, Sutter Instrument) onto a P-97 Flaming/Brown micropipette puller (Sutter Instrument). The pipette resistance was typically 3–6 MΩ after being filled with the intracellular solution. Since there were multiple layers of cells, we placed the pipette tip into the bath solution and focused on the tip. Once the pipette tip touched the target cells and formed a very small dimple, we released the positive pressure to obtain a GΩ seal. We then gave a small negative pressure to break through the membrane before recording according to our protocol. Briefly, the neurons were held at −70 mV to record the Na+/K+ channel activities with the voltage-clamp model. For recording action potentials, the cells were held at 0 pA with the current-clamp model, and with the steps of injected currents from −50 pA to + 50 pA. Spontaneous excitatory postsynaptic currents (sEPSCs) and spontaneous inhibitory postsynaptic currents (sIPSCs) were recorded in gap-free mode at a holding potential of -70 mV and 0 mV, respectively. sIPSCs were blocked by application of the GABAA receptor antagonist bicuculline (10 μM). For ChR2 stimulation, a light stimulation fiber was placed 5mm from the dish. A custom-made LED device (1 Watt, 470 nm; Cree lighting Inc.) coupled to a fiber optic cable was used to achieve the stimulation. EPSCs were recorded before the blue light stimulation(baseline), with blue light stimulation (30∼60 s, 470 nm, 0.4 mW/mm2) and after blue light stimulation under the voltage-clamp mode. mCherry-striatal neurons in printed cortico-striatal tissue were randomly selected for recordings. An Olympus BX51WI microscope was used to visualize neurons. A MultiClamp 700B amplifier (Axon instruments, Molecular Devices, Sunnyvale, CA, USA) was used to investigate the voltage clamp and current clamp recordings. Signals were filtered at 4 kHZ using a Digidata 1550B analog-digital converter (Axon instruments) and stored for further analysis. Data were analyzed with Clampfit 11.0.3 (Axon instruments), GraphPad Prism 5 (GraphPad Software Inc., La Jolla, CA, USA), CorelDraw 2019 (Corel, Canada), Igor 4.0 (WaveMetrics, Lake Oswego, OR, USA).

QUANTIFICATION AND STATISTICAL ANALYSIS

All data were expressed as mean ± standard deviation. Graphs and statistical analysis were made in GraphPad Prism. Distribution of the raw data was tested for normality of distribution; statistical analyses were performed using the t-test, or ANOVA tests as indicated.